

Note on Recursion Methods

Taisuke Ozaki

Research Institute for Computational Sciences (RICS),
National Institute of Advanced Industrial Science and Technology (AIST)
1-1-1 Umezono, Tsukuba, Ibaraki 305-8568, Japan

Jan 2003

Contents

1	Orthogonal Basis Sets	2
1.1	Theory	2
1.1.1	Tight-binding	2
1.1.2	One-particle Green's functions	4
1.1.3	Recursion method	6
1.1.4	Block recursion method	10
1.1.5	Moment description	16
1.1.6	Details on implementation	18
1.1.7	Analytic example	22
1.2	Convergence Properties	27
1.2.1	Energy convergence	28
1.2.2	Force convergence	30
1.2.3	Computational efficiency	32
2	Non-Orthogonal Basis Sets	35
2.1	Non-orthogonal basis sets	35
2.2	Algorithm A	36
2.2.1	Formalism	36
2.2.2	Analytic example	38
2.3	Algorithm B	40
2.3.1	Formalism	40
2.3.2	Analytic example	41
2.3.3	Numerical tests	43
2.4	Algorithm C	47
2.4.1	Formalism	47
2.5	Algorithm D	48
2.5.1	Formalism	48
2.6	Preliminary tests	49
A	Modified Matsubara Summation	50
	Bibliography	54

Chapter 1

Orthogonal Basis Sets

In this chapter, the theory of recursion methods are discussed within an orthogonal tight-binding representation. Then, as an extension of the recursion method, a practical recursion method based on the block Lanczos algorithm are presented. Several convergence properties for energies and forces show that the block scheme handles automatically the very different character of σ and π bonds by introducing block elements, which produces rapid convergence of the energies and forces within insulators, semiconductors, metals, and molecules. The method gives the first convergent results for vacancies in semiconductors using a moments-based method with a low number of moments. Our use of the Lanczos basis simplifies the calculations of the band energy and forces, which allows the application of the method to the molecular dynamics simulations of large systems.

1.1 Theory

1.1.1 Tight-binding

Let us start the recursion method or bond-order potential (BOP) within the two center orthogonal TB representation[10, 31]. It will be assumed that the basis set is an orthonormal set of atomiclike orbitals $|i\alpha\rangle$ where i is a site index, and α an orbital index. The Hamiltonian can be represented by the matrix $H_{i\alpha,j\beta} = \langle i\alpha|\hat{H}|j\beta\rangle$. The on-site elements of the matrix are written as $\epsilon_{i\alpha}$. The cohesive energy, assuming that the electrons are at a finite temperature T , is the sum of bond, promotion, and repulsive energies:

$$E_{\text{coh}} = E_{\text{bond}} + E_{\text{prom}} + E_{\text{rep}}, \quad (1.1)$$

where the repulsive energy is given by the sum of pair potentials or embedded potentials which are usually determined so that the TB model reproduces equilibrium structures and elastic constants. The bond energy is the attractive contribution that leads to cohesion. There are two different but equivalent expressions that describe the bond energy. The first gives the bond energy in terms of the *on-site* density of states as follows:

$$E_{\text{bond}} = 2 \sum_{i\alpha} \int (E - \epsilon_{i\alpha}) n_{i\alpha}(E) f\left(\frac{E - \mu}{k_B T}\right) dE, \quad (1.2)$$

where $n_{i\alpha}(E)$ is the density of states projected onto orbital $|i\alpha\rangle$, and the function $f(x) = 1/[1 + \exp(x)]$ is the Fermi function. The second gives the bond energy explicitly in terms

of the individual *intersite* bond energies as follows:

$$E_{\text{bond}} = \frac{1}{2} \sum_{i\alpha \neq j\beta} \left(2\Theta_{i\alpha, j\beta} H_{j\beta, i\alpha} \right), \quad (1.3)$$

where $\Theta_{i\alpha, j\beta}$ is the bond-order between orbitals $|i\alpha\rangle$ and $|j\beta\rangle$, and the expression parenthesis represents the corresponding bond energy associated with orbitals $|i\alpha\rangle$ and $|j\beta\rangle$. This allows us to interpret the bonding and structure of molecules and solids from a chemical point of view[32]. It should be noted that the bond-order is not pairwise but is determined by the particular arrangement and connectivity of the atoms adjacent to the two atoms forming the bond. In the block BOP representation the two different expressions Eqs. (1.2) and (1.3) for the bond energy are exactly identical at any level of approximations. The proof will be given later on. The promotion energy is defined by

$$E_{\text{prom}} = \sum_{i\alpha} \left(\epsilon_{i\alpha} N_{i\alpha} - \epsilon_{i\alpha}^0 N_{i\alpha}^0 \right), \quad (1.4)$$

where $N_{i\alpha}$ and $N_{i\alpha}^0$ are the number of electrons in $|i\alpha\rangle$ in the condensed and free atomic systems, respectively. The promotion energy is repulsive due to the excitation of electrons from their free atomic ground state as the atoms are brought together. Therefore, the cohesive energy of a system is determined by the balance between the attractive bond energy and the repulsive pairwise/embedding and promotion energies. The bond and promotion energies can be repartitioned into the band and atomic energies:

$$\begin{aligned} E_{\text{bond}} + E_{\text{prom}} &= \sum_{i\alpha \neq j\beta} \Theta_{i\alpha, j\beta} H_{j\beta, i\alpha} + \sum_{i\alpha} \left(\epsilon_{i\alpha} N_{i\alpha} - \epsilon_{i\alpha}^0 N_{i\alpha}^0 \right) \\ &= \sum_{i\alpha, j\beta} \Theta_{i\alpha, j\beta} H_{j\beta, i\alpha} - \sum_{i\alpha} \epsilon_{i\alpha}^0 N_{i\alpha}^0 \\ &= E_{\text{band}} - E_{\text{atoms}}. \end{aligned} \quad (1.5)$$

E_{band} is equal to the energy which is defined by integrating $\sum_{i\alpha} E n_{i\alpha}(E)$ up to the Fermi level.

In the TB model the single particle eigenfunctions are expanded in a basis set that is an orthonormal set of real atomiclike orbitals: $|i\alpha\rangle$.

$$|\phi\rangle = \sum_{i\alpha} C_{i\alpha}^{(\phi)} |i\alpha\rangle, \quad (1.6)$$

where the expansion coefficients are defined by $C_{i\alpha}^{(\phi)} \equiv \langle i\alpha | \phi \rangle$. $C_{i\alpha}^{(\phi)}$ is always real because of real atomic orbitals and Hamiltonian. Then the bond-orders may be defined in terms of the expansion coefficients as follows:

$$\Theta_{i\alpha, j\beta} = 2 \sum_{\phi} C_{j\beta}^{(\phi)} C_{i\alpha}^{(\phi)} f \left(\frac{\epsilon^{(\phi)} - \mu}{k_B T} \right), \quad (1.7)$$

where the factor 2 accounts for spin degeneracy. $\epsilon^{(\phi)}$ is the eigenvalue corresponding to an eigenstate $|\phi\rangle$.

The force on atom k is obtained by differentiating Eq. (1.1) with respect to atomic positions:

$$\begin{aligned}\mathbf{F}_k &= -\frac{\partial E_{\text{coh}}}{\partial \mathbf{r}_k} \\ &= -\sum_{i\alpha, j\beta} \left(\frac{\partial \Theta_{i\alpha, j\beta}}{\partial \mathbf{r}_k} H_{j\beta, i\alpha} + \Theta_{i\alpha, j\beta} \frac{\partial H_{j\beta, i\alpha}}{\partial \mathbf{r}_k} \right) - \frac{\partial E_{\text{rep}}}{\partial \mathbf{r}_k}.\end{aligned}\quad (1.8)$$

The first term of Eq. (1.8) is identically zero at zero electronic temperature so that

$$\mathbf{F}_k = -\sum_{i\alpha, j\beta} \Theta_{i\alpha, j\beta} \frac{\partial H_{j\beta, i\alpha}}{\partial \mathbf{r}_k} - \frac{\partial E_{\text{rep}}}{\partial \mathbf{r}_k}, \quad (1.9)$$

where the first term of Eq. (1.9) is the Hellmann-Feynman force. If the bond-orders are approximate values, then the sum of the derivatives of the bond-orders with respect to atomic positions will not be zero, so that Eq. (1.9) gives the exact force which is consistent with the total energy at zero temperature. while in insulators and metals at a finite temperature, on the other hand, the sum is not always zero. However, in the block BOP representation the forces are given by Eq. (1.9), since it is very difficult to evaluate the derivatives of the bond-orders. Hence, the forces calculated by block BOP become exact as the bond-orders converge to the exact values.

1.1.2 One-particle Green's functions

The local density of states and bond-orders can be related to the one particle Green's functions. The one particle Green's function operator is defined by

$$\begin{aligned}\hat{G}(Z) &= (Z - \hat{H})^{-1} \\ &= \sum_{\phi} \frac{|\phi\rangle\langle\phi|}{Z - \epsilon^{(\phi)}}.\end{aligned}\quad (1.10)$$

Then the imaginary part of the diagonal elements of the Green's function matrix give the local density of states:

$$\begin{aligned}\text{Im } G_{i\alpha, i\alpha}(E + i0^+) &= \sum_{\phi} \frac{-0^+ \langle i\alpha | \phi \rangle \langle \phi | i\alpha \rangle}{(E - \epsilon^{(\phi)})^2 + (0^+)^2} \\ &= -\pi \sum_{\phi} (C_{i\alpha}^{(\phi)})^2 \delta(E - \epsilon^{(\phi)}) \\ &= -\pi n_{i\alpha}(E).\end{aligned}$$

Therefore

$$n_{i\alpha}(E) = -\frac{1}{\pi} \text{Im } G_{i\alpha, i\alpha}(E + i0^+), \quad (1.11)$$

where $G_{i\alpha, i\alpha}(Z) = \langle i\alpha | \hat{G}(Z) | i\alpha \rangle$, 0^+ represents a positive infinitesimal, and $\delta(x)$ is the delta function. The imaginary part of the off-diagonal elements of the Green's function matrix has the following relation to the expansion coefficients of the single particle eigenfunctions:

$$\text{Im } G_{i\alpha, j\beta}(E + i0^+) = -\pi \sum_{\phi} C_{j\beta}^{(\phi)} C_{i\alpha}^{(\phi)} \delta(E - \epsilon^{(\phi)}). \quad (1.12)$$

Multiplying the both sides of Eq. (1.12) by the Fermi function, integrating with respect to the energy we obtain the following useful expression for the bond-order:

$$\begin{aligned}
& \text{Im} \int G_{i\alpha,j\beta}(E + i0^+) f\left(\frac{E - \mu}{k_B T}\right) dE \\
&= -\pi \sum_{\phi} C_{j\beta}^{(\phi)} C_{i\alpha}^{(\phi)} \int \delta(E - \epsilon^{(\phi)}) f\left(\frac{E - \mu}{k_B T}\right) dE \\
&= -\pi \sum_{\phi} C_{j\beta}^{(\phi)} C_{i\alpha}^{(\phi)} f\left(\frac{\epsilon^{(\phi)} - \mu}{k_B T}\right) \\
&= -\frac{\pi}{2} \Theta_{i\alpha,j\beta}.
\end{aligned}$$

Therefore

$$\Theta_{i\alpha,j\beta} = -\frac{2}{\pi} \text{Im} \int G_{i\alpha,j\beta}(E + i0^+) f\left(\frac{E - \mu}{k_B T}\right) dE. \quad (1.13)$$

The evaluations of the bond energy Eqs. (1.2) and (1.3) require calculating the local density of states and bond-orders. We obtain the local density of states and bond-orders from the Green's function through Eqs. (1.11) and (1.13). The diagonal elements of the Green's function matrix can be calculated in a numerically stable way by the recursion method[33, 34].

Additional derivation (A)

Consider the matrix form of Green's function:

$$G(Z) = (ZI - H)^{-1}$$

The Hamiltonian H follows the eigenvalue matrix equation:

$$HA = AE$$

Then

$$\begin{aligned}
G(Z) &= (ZI - HAA^\dagger)^{-1} \\
&= (ZI - AEA^\dagger)^{-1} \\
&= (ZAA^\dagger - AEA^\dagger)^{-1} \\
&= (A[ZI - E]A^\dagger)^{-1} \\
&= (A[ZI - E]^{-1}A^\dagger)
\end{aligned}$$

So, we have

$$G_{ij}(Z) = \sum_{k=1}^N a_{ik} a_{jk}^*$$

Additional derivation (B)

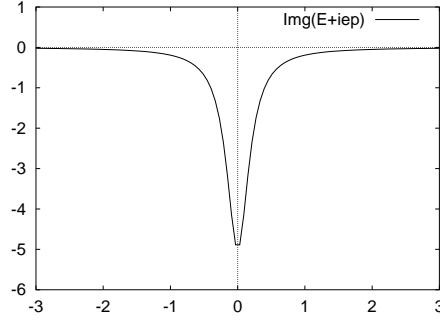
Let us consider the nature of a function $g(Z)$:

$$g(Z) = \frac{1}{Z - E_0}$$

Let Z be $E + i\varepsilon$, then

$$\begin{aligned} \text{Img}(E + i\varepsilon) &= \frac{1}{2i} \left(\frac{1}{Z - E_0} - \frac{1}{Z^* - E_0} \right) \\ &= \frac{1}{2i} \left(\frac{1}{E - E_0 + i\varepsilon} - \frac{1}{E - E_0 - i\varepsilon} \right) \\ \text{Img}(E + i\varepsilon) &= \frac{-\varepsilon}{(E - E_0)^2 + \varepsilon} \end{aligned}$$

Outline of $\text{Img}(E + i\varepsilon)$ are as follows:



where $E_0 = 0$ and $\varepsilon = 0.2$. Integrating $\text{Img}(E + i\varepsilon)$ on the real axis:

$$\begin{aligned} \int_{-\infty}^{\infty} \text{Img}(E + i\varepsilon) dE &= \int_{-\infty}^{\infty} \frac{-\varepsilon}{(E - E_0)^2 + \varepsilon} \\ &= -\varepsilon \left[\frac{1}{\varepsilon} \tan^{-1} \frac{E - E_0}{\varepsilon} \right]_{-\infty}^{\infty} \\ &= -\pi \end{aligned}$$

So, we find

$$\lim_{\varepsilon \rightarrow 0} -\frac{1}{\pi} \text{Img}(E + i\varepsilon) = \delta(E - E_0)$$

1.1.3 Recursion method

Any Hermite Hamiltonian matrix H can be tridiagonalized using the Lanczos algorithm. First, assume that H is tridiagonalized by the unitary transformation with an unitary matrix U :

$$H_{\text{TD}} = U^\dagger H U. \quad (1.14)$$

H and H_{TD} are satisfied the following eigenvalue matrix equations:

$$HA = AE, \quad (1.15)$$

$$H_{\text{TD}}B = BE. \quad (1.16)$$

So, we have $B = U^\dagger A$. The Green's function $G_{\text{TD}}(Z)$ for H_{TD} can be related to the original Green's function $G(Z)$ as follows:

$$\begin{aligned} G_{\text{TD}}(Z) &= (ZI - H_{\text{TD}})^{-1}, \\ &= (ZI - U^\dagger H U)^{-1}, \\ &= (ZU^\dagger U - U^\dagger H U)^{-1}, \\ &= [U^\dagger (ZI - H) U]^{-1}, \\ &= U^\dagger (ZI - H)^{-1} U, \\ G_{\text{TD}}(Z) &= U^\dagger G(Z) U. \end{aligned} \quad (1.17)$$

Also, the diagonal elements $G_{ii}(Z)$ and $G_{ii}^{\text{TD}}(Z)$ are written using A and B , respectively, as follows:

$$G_{ii}(Z) = \sum_{k=1}^N a_{ik} a_{jk}^* \frac{1}{Z - E_k} \quad (1.18)$$

$$G_{ii}^{\text{TD}}(Z) = \sum_{k=1}^N b_{ik} b_{jk}^* \frac{1}{Z - E_k}. \quad (1.19)$$

Here, let us assume that $G_{ii}^{\text{TD}}(Z)$ is equivalent to $G_{ii}(Z)$. The assumption requires $a_{ij} = b_{ij}$. Considering $a_{ij} = \sum_{k=1}^N u_{ik} b_{kj}$, then, the following condition must be satisfied:

$$\begin{aligned} u_{ik} &= 1 & k = i \\ u_{ik} &= 0 & k \neq i \end{aligned} \quad (1.20)$$

By the Lanczos algorithm, we can make an unitary matrix which satisfies the condition Eq. (1.20). Writing Eq. (1.14) explicitly, we have

$$H\{|u_0 \rangle, |u_1 \rangle, |u_2 \rangle, \dots, |u_N \rangle\} = \{|u_0 \rangle, |u_1 \rangle, |u_2 \rangle, \dots, |u_N \rangle\} \times \begin{pmatrix} \alpha_0 & \beta_1 & & & & \\ \beta_1 & \alpha_1 & \beta_2 & & & \\ & \dots & \dots & & & \\ & & \dots & \dots & & \\ & & & \beta_{N-1} & \alpha_{N-1} & \beta_N \\ & & & & \beta_N & \alpha_N \end{pmatrix}, \quad (1.21)$$

$$\begin{aligned} H|u_0 \rangle &= |u_0 \rangle \alpha_0 + |u_1 \rangle \beta_1, \\ H|u_1 \rangle &= |u_0 \rangle \beta_1 + |u_1 \rangle \alpha_1 + |u_2 \rangle \beta_2, \\ &\dots \\ H|u_n \rangle &= |u_{n-1} \rangle \beta_n + |u_n \rangle \alpha_n + |u_{n+1} \rangle \beta_{n+1}, \end{aligned} \quad (1.22)$$

where $U = \{|u_0 \rangle, |u_1 \rangle, |u_2 \rangle, \dots, |u_N \rangle\}$. Then, inversely solving Eq. (1.22), we get the following Lanczos algorithm:

$$\begin{aligned}
&\text{Set} && \langle u_0 | = (1, 0, 0, \dots) \\
&\text{Compute} && H|u_n \rangle \\
&\text{Compute} && \alpha_n = \langle u_n | H|u_n \rangle \\
&\text{Compute} && |r_n \rangle = H|u_n \rangle - |u_{n-1} \rangle \beta_n - |u_n \rangle \alpha_n \\
&\text{Compute} && \beta_n = \sqrt{\langle r_n | r_n \rangle} \\
&\text{Compute} && |u_{n+1} \rangle = |r_n \rangle / \beta_n \\
&&& n := n + 1
\end{aligned} \tag{1.23}$$

It can be easily proven by the inductive method that $U = \{|u_0 \rangle, |u_1 \rangle, |u_2 \rangle, \dots, |u_N \rangle\}$ is an orthonormal set. From Eq. (1.23), we have

$$|u_{n+1} \rangle \beta_n = H|u_n \rangle - |u_{n-1} \rangle \beta_n - |u_n \rangle \alpha_n \tag{1.24}$$

In case of $n = 0$, $\langle u_0 | u_0 \rangle = 1$. Assuming that $\{|u_n \rangle\}$ is an orthonormal set upto n , then Multiplying $\langle u_k |$ for $k = 0 \sim n$ from the left side of Eq. (1.24), we find

$$\begin{aligned}
\langle u_k | u_{n+1} \rangle \beta_n &= \langle u_k | H|u_n \rangle - \langle u_k | u_{n-1} \rangle \beta_n - \langle u_k | u_n \rangle \alpha_n \\
&= 0.
\end{aligned} \tag{1.25}$$

In case of $k = n + 1$, we clearly see $\langle u_{n+1} | u_{n+1} \rangle = 1$. Therefore, $U = \{|u_0 \rangle, |u_1 \rangle, |u_2 \rangle, \dots, |u_N \rangle\}$ is an orthonormal set.

We also find that the condition, Eq. (1.20), is satisfied for $U = \{|u_0 \rangle, |u_1 \rangle, |u_2 \rangle, \dots, |u_N \rangle\}$. So, we can use $G_{00}^{\text{TD}}(Z)$ instead of $G_{ii}(Z)$. $G_{00}^{\text{TD}}(Z)$ is calculated as the ratio of the determinant D to the reduced determinant D_1 of $(ZI - H_{\text{TD}})$ as follows:

$$G_{00}^{\text{TD}}(Z) = \frac{D_1}{D} \tag{1.26}$$

where

$$D = \det(ZI - H_{\text{TD}}) \tag{1.27}$$

$$D_1 = \det(ZI - H'_{\text{TD}}) \tag{1.28}$$

with

$$H'_{\text{TD}} = \begin{pmatrix} \alpha_1 & \beta_2 & & & & \\ \beta_2 & \alpha_2 & \beta_3 & & & \\ & \cdots & \cdots & & & \\ & & \cdots & \cdots & & \\ & & & \beta_{N-1} & \alpha_{N-1} & \beta_N \\ & & & & \beta_N & \alpha_N \end{pmatrix},$$

Let us consider Cauchy expansion, the determinants D and D_n for the tridiagonaized Hamiltonian H_{TD} .

$$\begin{pmatrix} \alpha_0 & \beta_1 & & & \\ \beta_1 & \alpha_1 & \beta_2 & & \\ & \cdots & \cdots & \cdots & \\ & & \cdots & \cdots & \\ & & & \beta_{N-1} & \alpha_{N-1} & \beta_N \\ & & & & \beta_N & \alpha_N \end{pmatrix}, \quad (1.29)$$

$\det(ZI - H_{\text{TD}})$ can be written using Laplace expansion for the first row as follows:

$$\det(ZI - H_{\text{TD}}) = (Z - \alpha_0)A_{11} - \beta_1 A_{12}, \quad (1.30)$$

where A_{11} and A_{12} are cofactors given by

$$A_{11} = D_1, \quad (1.31)$$

$$A_{12} = \beta_1 D_2. \quad (1.32)$$

Therefore, we have

$$D = (Z - \alpha_0)D_1 - \beta_1^2 D_2 \quad (1.33)$$

Generalizing the above equation, we can write as

$$D_n = (Z - \alpha_n)D_{n+1} - \beta_{n+1}^2 D_{n+2} \quad (1.34)$$

Using the relation, Eq. (1.34), we rewrite Eq. (1.26) in a continued fraction as follows:

$$\begin{aligned} G_{00}^L(Z) &= \frac{D_1}{D} \\ &= \frac{D_1}{(Z - \alpha_0)D_1 - \beta_1^2 D_2} \\ &= \frac{1}{Z - \alpha_0 - \frac{\beta_1^2 D_2}{D_1}} \\ &= \frac{1}{Z - \alpha_0 - \frac{\beta_1^2 D_2}{(Z - \alpha_1)D_2 - \beta_2^2 D_3}} \\ &\dots \\ G_{00}^L(Z) &= \frac{1}{Z - \alpha_0 - \frac{\beta_1^2}{Z - \alpha_1 - \frac{\beta_2^2}{Z - \alpha_2 - \frac{\beta_3^2}{\ddots}}}}. \end{aligned} \quad (1.35)$$

Next, we consider terminating the continued fraction. Assuming that α_n and β_n for $N_t \leq n$ are constant, The terminator $T(Z)$ can be written by a closed form including itself as follows:

$$T(Z) = \frac{1}{Z - \alpha_\infty - \frac{\beta_\infty^2}{Z - \alpha_\infty - \frac{\beta_\infty^2}{Z - \alpha_\infty - \frac{\beta_\infty^2}{\ddots}}}}$$

$$T(Z) = \frac{1}{Z - \alpha_\infty - \beta_\infty^2 T(Z)} \quad (1.36)$$

If we solve Eq. (1.36) regarding $T(Z)$, then we get a well known square root terminator:

$$T(Z) = \frac{(Z - \alpha_\infty - \sqrt{(Z - \alpha_\infty)^2 - 4\beta_\infty^2})}{4\beta_\infty^2} \quad (1.37)$$

1.1.4 Block recursion method

Block BOP is a general recursion method for evaluating efficiently both the diagonal and off-diagonal elements of the Green's function matrix by the recursion method. The first step of the recursion method is to tridiagonalize the Hamiltonian using the Lanczos algorithm[35]. In the block BOP we introduce the *block* Lanczos algorithm with the starting state as a single site containing all the valence orbitals rather than the usual *scalar* Lanczos algorithm with a single starting orbital[13]. However, the application of the conventional block algorithm[36, 37] to finite systems such as molecules introduces a numerical instability, since the terminal number of recursion levels of the π bond are different from that of the σ bond in the recursive algorithm. Therefore, we modify the conventional block Lanczos algorithm. A series of procedures for the modified block Lanczos algorithm can be carried out as follows:

$$|U_0\rangle = (|i1\rangle, |i2\rangle, \dots, |iM_i\rangle). \quad (1.38)$$

$$\underline{A}_n = (U_n | \hat{H} | U_n). \quad (1.39)$$

$$|r_n\rangle = \hat{H}|U_n\rangle - |U_{n-1}\rangle {}^t \underline{B}_n - |U_n\rangle \underline{A}_n. \quad (1.40)$$

$$(\underline{B}_{n+1})^2 = (r_n | r_n). \quad (1.41)$$

$$(\underline{\lambda}_n)^2 = {}^t \underline{V}_n (\underline{B}_{n+1})^2 \underline{V}_n. \quad (1.42)$$

$$\underline{B}_{n+1} = \underline{\lambda}_n {}^t \underline{V}_n. \quad (1.43)$$

$$(\underline{B}_{n+1})^{-1} = \underline{V}_n \underline{\lambda}_n^{-1}. \quad (1.44)$$

$$|U_{n+1}\rangle = |r_n\rangle (\underline{B}_{n+1})^{-1}. \quad (1.45)$$

\underline{A}_n and \underline{B}_n are recursion block coefficients with $M_i \times M_i$ in size, where M_i is the number of atomic orbitals on the starting atom i , and the underline indicates that the element is a block.

The states $|U_n\rangle = (|L_{n1}\rangle, |L_{n2}\rangle, \dots, |L_{nM_i}\rangle)$ represent the Lanczos basis, and are orthonormal and block-tridiagonalize the Hamiltonian. The modified algorithm gives different

expressions for the block elements \underline{B}_{n+1} and these inverses compared with the conventional algorithm. The block elements in the conventional block Lanczos algorithm are defined by

$$\underline{B}_{n+1} = \underline{V}_n \underline{\lambda}_n {}^t \underline{V}_n. \quad (1.46)$$

$$(\underline{B}_{n+1})^{-1} = \underline{V}_n \underline{\lambda}_n^{-1} {}^t \underline{V}_n. \quad (1.47)$$

The failure in the conventional algorithm can be illustrated by a carbon trimer with a linear chain structure along the x -axis. If the block Lanczos algorithm is applied with the central atom in the trimer as the starting state, then the p_y and p_z orbitals span two independent subspaces. Thus, the recursive algorithm finishes after only one iteration for the Lanczos vectors concerned with the p_y and p_z orbitals. This gives two zero eigenvalues in the four eigenvalues of the block element $(\underline{B}_2)^2$. Then one can not evaluate the inverse of \underline{B}_2 using Eq. (1.44). Therefore, defining \underline{B}_2 and its inverse by the modified Eqs. (1.48) and (1.49), respectively, and assuming that the diagonal elements of $\underline{\lambda}_1^{-1}$ corresponding to the zero eigenvalues are zero we have

$$\underline{B}_2(\underline{B}_2)^{-1} = \begin{pmatrix} 1 & & & \\ & 1 & & \\ & & 0 & \\ & & & 0 \end{pmatrix}. \quad (1.48)$$

$$(\underline{U}_2 | \underline{U}_2) = \begin{pmatrix} 1 & & & \\ & 1 & & \\ & & 0 & \\ & & & 0 \end{pmatrix}. \quad (1.49)$$

$|\underline{U}_2\rangle$ is reduced to the state with two vectors, while the starting state $|\underline{U}_0\rangle$ is constructed by the four vectors, which permits us to iterate once more with the recursive algorithm. The conventional block Lanczos algorithm does not satisfy both Eqs. (1.48) and (1.49), since the block elements \underline{B}_2 and the inverse are obtained from the unitary transformations of $\underline{\lambda}_1$ and the inverse, respectively. Therefore, the conventional algorithm terminates at this recursion level even though the Lanczos vectors for the σ orbital can still hop. This reduction of the state avoids the numerical instabilities for the case of small eigenvalues of $(\underline{B}_{n+1})^2$, even when the eigenvalues are not zero.

Application of the block Lanczos algorithm defines an orthonormal basis set called the Lanczos vector or basis. The Lanczos vectors reflect the neighboring atomic arrangement of the starting site. In Fig. 1.1 we show the Lanczos vectors on an s -valent square lattice. The Lanczos vectors spread gradually from the central atom as the number of recursion levels increases. Thus, we now expand a one electron eigenstate using the Lanczos vectors:

$$|\phi\rangle = \sum_{n\nu} D_{n\nu}^{(\phi)} |L_{n\nu}\rangle, \quad (1.50)$$

where $D_{n\nu}^{(\phi)} \equiv \langle L_{n\nu} | \phi \rangle$. Then the representation based on the atomic basis can be transformed into that of the Lanczos basis set by the matrix U such that

$$T^L = {}^t U T U, \quad (1.51)$$

matrix. In the block BOP the bond-orders are evaluated in the Lanczos basis representation, and then we get the bond-orders based on the atomic basis from Eq. (1.52).

It is essential to start the block Lanczos algorithm with a single site as in Eq. (1.38). Although it is possible to derive an analogous transformation to Eq. (1.52) using the usual scalar Lanczos algorithm, the bond energy of the system depends on the rotation of the system[37]. Thus, the use of the scalar algorithm is not appropriate, since the bond energy should be invariant to the rotation of the system. We could also start the recursion with a cluster containing a neighbor shell of atoms instead of a single site[36]. However, this choice is unsuitable because it is highly computationally intensive.

In the Lanczos representation the Hamiltonian is block-tridiagonalized:

$$(U_m|\hat{H}|U_n) = \begin{cases} \underline{A}_n & \text{if } m = n, \\ {}^t\underline{B}_n & \text{if } m = n - 1, \\ \underline{B}_{n+1} & \text{if } m = n + 1, \\ \underline{0} & \text{otherwise.} \end{cases} \quad (1.55)$$

The block element $\underline{G}_{00}(Z) = (U_0|\hat{G}|U_0)$ can be written explicitly by the form of the multiple inverse, since the Green's function matrix $G(Z)$ is the inverse of the matrix $(ZI - H)$. Applying repeatedly the partitioning method[38, 39], which is a method for calculating the inverse of matrices, to the matrix $(ZI - H)$ we get

$$\underline{G}_{00}^L(Z) = [ZI - \underline{A}_0 - {}^t\underline{B}_1[ZI - \underline{A}_1 - {}^t\underline{B}_2[\dots]^{-1}\underline{B}_2]^{-1}\underline{B}_1]^{-1}. \quad (1.56)$$

$\underline{G}_{00}^L(Z)$ is equal to the block element $\underline{G}_{ii}(Z)$ based on the atomic basis, since we have started the block Lanczos algorithm with Eq. (1.38). Therefore, the local density of states can be evaluated from the diagonal elements by Eq. (1.11). Also the trace of $\underline{G}_{00}^L(Z)$ gives the local density of states on atom i .

Moreover, by taking account of the block-tridiagonalized Hamiltonian and the identity $(ZI - H)G(Z) = \mathbf{I}$ in the Lanczos basis representation, the off-diagonal elements of the Green's function matrix \underline{G}_{0n}^L may be obtained from the following recurrence relation:

$$\underline{G}_{0n}^L(Z) = \left(\underline{G}_{0n-1}^L(Z)(ZI - \underline{A}_{n-1}) - \underline{G}_{0n-2}^L(Z){}^t\underline{B}_{n-1} - \delta_{1n}\mathbf{I} \right) (\underline{B}_n)^{-1}, \quad (1.57)$$

where δ is the Kronecker's delta, $\underline{G}_{0-1}(Z)$ and ${}^t\underline{B}_0$ are $\underline{0}$, respectively. All the off-diagonal block elements $\underline{G}_{0n}^L(Z)$ are related to the diagonal block element $\underline{G}_{00}^L(Z)$. Once $\underline{G}_{00}^L(Z)$ has been obtained, the off-diagonal block elements are easily evaluated from the above recursive relation. The simplicity of evaluating the off-diagonal block elements is an important advantage of the Lanczos basis representation. The block elements of the Green's function matrix have the same relation to the bond-orders based on the Lanczos basis as that of the atomic basis representation:

$$\underline{\Theta}_{0n}^L = -\frac{2}{\pi} \text{Im} \int \underline{G}_{0n}^L(E + i0^+) f\left(\frac{E - \mu}{k_B T}\right) dE \quad (1.58)$$

In case the bond-orders are evaluated by Eqs. (1.52) and (1.58), we can prove that the two different expressions Eqs. (1.2) and (1.3) for the bond energy are identical at any level of approximations. Consider the trace of $G(Z)(ZI - H)$. Transforming the trace of the atomic

basis representation into that of the Lanczos basis using Eq. (1.51), and making use of the identity $G(Z)(ZI - H) = I$ in the Lanczos basis representation we see that the trace is a constant:

$$\begin{aligned}
& \text{tr} \{G(Z)(ZI - H)\} \\
&= \sum_i \text{tr} \{Z\underline{G}_{ii}(Z)\} - \sum_{ij} \text{tr} \{\underline{G}_{ij}(Z)\underline{H}_{ji}\} \\
&= \sum_i \text{tr} \{Z\underline{G}_{00}^{L^{(i)}}(Z)\} - \sum_{in} \text{tr} \{\underline{G}_{0n}^{L^{(i)}}(Z)\underline{H}_{n0}^{L^{(i)}}\} \\
&= \sum_i \text{tr}(\underline{I}^{(i)}), \tag{1.59}
\end{aligned}$$

where \underline{I}_i is a unit matrix with $M_i \times M_i$ in size. The index $L^{(i)}$ indicates the representation based on the Lanczos basis with the starting state on atom i . Considering the imaginary parts of the trace we have

$$\text{Im} \sum_{i\alpha} ZG_{i\alpha,i\alpha}(Z) = \text{Im} \sum_{i\alpha,j\beta} G_{i\alpha,j\beta}(Z)H_{j\beta,i\alpha}. \tag{1.60}$$

We see that the two expressions for the bond energy give the same energy, since the Green's functions can be related to the local density of states and bond-orders through Eqs. (1.11) and (1.13), respectively. The block BOP, thus, provides the equivalence of the two expressions for the bond energy in a natural way, whereas in the usual BOP the Green's functions need a carefully chosen truncator in order to satisfy the sum rule[12].

Additional derivation (C)

The derivation of Eq. (1.56) is given here. Let us introduce the partitioning method for inverting a matrix. We divide a matrix, A , with the size $N \times N$ into $A_1(p \times p)$, $A_2(p \times q)$, $A_3(q \times p)$, and $A_4(q \times q)$, where $N = p + q$ as follows:

$$A = \begin{pmatrix} A_1 & A_2 \\ A_3 & A_4 \end{pmatrix} \tag{C.1}$$

Similarly, we write the inverse A^{-1} as

$$A^{-1} = \begin{pmatrix} X_1 & X_2 \\ X_3 & X_4 \end{pmatrix} \tag{C.2}$$

Taking into account $AA^{-1} = I$, the following equations are derived:

$$AA^{-1} = \begin{pmatrix} A_1 & A_2 \\ A_3 & A_4 \end{pmatrix} \begin{pmatrix} X_1 & X_2 \\ X_3 & X_4 \end{pmatrix} = \begin{pmatrix} A_1X_1 + A_2X_3 & A_1X_2 + A_2X_4 \\ A_3X_1 + A_4X_3 & A_3X_2 + A_4X_4 \end{pmatrix} = I$$

$$A_1X_1 + A_2X_3 = I \tag{C.3}$$

$$A_1X_2 + A_2X_4 = 0 \tag{C.4}$$

$$A_3X_1 + A_4X_3 = 0 \quad (C.5)$$

$$A_3X_2 + A_4X_4 = I \quad (C.6)$$

Then, considering Eq. (C.3) - $A_2A_4^{-1} \times$ Eq. (C.5), we have

$$(A_1 - A_2A_4^{-1}A_3)X_1 = I$$

Here, replacing

$$\Delta = A_1 - A_2A_4^{-1}A_3 \quad (C.7)$$

Then, we have

$$X_1 = \Delta^{-1} \quad (C.8)$$

Returning back Eq. (C.5),

$$\begin{aligned} A_4X_3 &= -A_3X_1 \\ X_3 &= -A_4^{-1}A_3\Delta^{-1} \end{aligned} \quad (C.9)$$

Next, considering Eq. (C.4) - $A_2A_4^{-1} \times$ Eq. (C.6), we have

$$X_2 = -\Delta^{-1}A_2A_4^{-1} \quad (C.10)$$

From Eq. (C.6), we find

$$X_4 = A_4^{-1} - A_4^{-1}A_3X_2 \quad (C.11)$$

So, we see

$$X_1 = \Delta^{-1} \quad (C.8)$$

$$X_2 = -\Delta^{-1}A_2A_4^{-1} \quad (C.10)$$

$$X_4 = A_4^{-1} - A_4^{-1}A_3X_2 \quad (C.11)$$

$$\Delta = A_1 - A_2A_4^{-1}A_3 \quad (C.7)$$

From Eqs. (C.7) and (C.8), we have

$$X_1 = [A_1 - A_2A_4^{-1}A_3]^{-1} \quad (C.12)$$

Moreover, we apply the above treatment to the matrix A_4 . Similarly, dividing A_4 , we write

$$A_4 = \begin{pmatrix} B_1 & B_2 \\ B_3 & B_4 \end{pmatrix} \quad (C.13)$$

Similarly, we write the inverse

$$A_4^{-1} = \begin{pmatrix} Y_1 & Y_2 \\ Y_3 & Y_4 \end{pmatrix} \quad (C.14)$$

Applying the same procedure to A_4 , immediately, we find

$$Y_1 = [B_1 - B_2B_4^{-1}B_3]^{-1} \quad (C.15)$$

Similarly, the procedure can be applied to B_4 . So, we see that the diagonal block element $\underline{G}_{00}^L(Z)$ can be written in a multiple inverse.

This relation means that the imaginary part of the moment of the block diagonal element in the Green's function matrix is equal to the moment of the Hamiltonian.

Let us define the orthogonal block polynomials $\underline{P}_n(x)$:

$$x\underline{P}_n(x) = \underline{P}_n(x)\underline{A}_n + \underline{P}_{n-1}(x)^t\underline{B}_n + \underline{P}_{n+1}(x)\underline{B}_{n+1}, \quad (1.67)$$

where $\underline{P}_{-1}(x)$ and $\underline{P}_0(x)$ are the zero matrix $\underline{0}$ and the the unit matrix \underline{I} with $M_i \times M_i$ in size. By using the block polynomials the recursion block elements \underline{A}_n and \underline{B}_n can be expanded with the moments:

$$\begin{aligned} \underline{A}_n &= (U_n|H|U_n) \\ &= {}^t\underline{P}_n(\hat{H})(U_0|\hat{H}|U_0)\underline{P}_n(\hat{H}) \\ &= \sum_m^{2n+1} \underline{a}_m \underline{\mu}_{00}^{(m)} \underline{a}'_m. \end{aligned} \quad (1.68)$$

$$\begin{aligned} \underline{B}_n &= (U_n|H|U_{n-1}) \\ &= {}^t\underline{P}_n(\hat{H})(U_0|\hat{H}|U_0)\underline{P}_{n-1}(\hat{H}) \\ &= \sum_m^{2n} \underline{b}_m \underline{\mu}_{00}^{(m)} \underline{b}'_m. \end{aligned} \quad (1.69)$$

In the derivations of Eqs. (1.68) and (1.69) we have assumed the substitution: $|U_0\rangle\hat{H} \rightarrow \hat{H}|U_0\rangle$ and $\hat{H}(U_0| \rightarrow (U_0|\hat{H}$. The block coefficients \underline{a}_m , \underline{a}'_m , \underline{b}_m , and \underline{b}'_m are given by the recursion block elements. For example \underline{A}_1 and \underline{B}_1 can be written as follows:

$$\underline{A}_1 = ({}^t\underline{B}_1)^{-1} \left\{ \underline{\mu}_{00}^{(3)} - \underline{A}_0 \underline{\mu}_{00}^{(2)} - \underline{\mu}_{00}^{(2)} \underline{A}_0 + \underline{A}_0 \underline{\mu}_{00}^{(1)} \underline{A}_0 \right\} (\underline{B}_1)^{-1}. \quad (1.70)$$

$$\underline{B}_1 = ({}^t\underline{B}_1)^{-1} \left\{ \underline{\mu}_{00}^{(2)} - \underline{A}_0 \underline{\mu}_{00}^{(1)} \right\}. \quad (1.71)$$

In case the recursion in the block Lanczos algorithm is terminated at the q th level, the diagonal block element of the Green's function matrix can be expanded with the $(2q+1)$ th moments, because it is constructed by the multiple inverse with the recursion block elements $\underline{A}_n (n=0 \sim q)$, $\underline{B}_n (n=1 \sim q)$ given by the q th recursion. As shown in Eqs. (1.68) and (1.69), the recursion block elements are expanded in terms of the moments. Thus, \underline{G}_{00}^L contains the $0 \sim (2q+1)$ th moments. This implies that up to $(2q+1)$ th moment is included in the sum of the moment expansion Eq. (1.61), and Eq. (1.66) satisfies for $r \leq 2q+1$.

To obtain the moments for the off-diagonal elements of the Green's function matrix, multiplying both sides in Eq. (1.61) by $(E+0^+)^r$ and integrating with respect to the energy E , we have

$$\text{Im} \int_{-\infty}^{\infty} E^r \underline{G}_{0n}^L(E+0^+) dE = \sum_{m=0}^n \left(\text{Im} \int_{-\infty}^{\infty} E^{r+m} \underline{G}_{00}^L(E+0^+) dE \right) \underline{c}_m, \quad (1.72)$$

where the block coefficients \underline{c}_m can be written in terms of the recursion block elements. As mentioned above the right side of Eq. (1.72) is equal to the moment of the Hamiltonian for $r+m \leq 2q+1$, so that the left side gives the exact moment $\underline{\mu}_{0n}^{(r)}$ for $r \leq 2q+1-n$. This means that the off-diagonal elements of the Green's function matrix can be expanded

with up to the $(2q + 1 - n)$ th moment, which results in the expansion of the bond-order Θ_{0n}^L by up to the $(2q + 1 - n)$ th moment. Moreover we can relate the bond-orders in the atomic basis representation to the moments through the transformation Eq. (1.52). In the right side of Eq. (1.52) the bond-order Θ_{0q}^L for $n = q$ determines the maximum order of the moments for the bond-orders based on the atomic basis. So we see that the bond-orders in the atomic basis representation can be expanded with the moments for $r \leq q + 1$. Thus, in the block BOP the off-diagonal elements of the Green's function matrix can be constructed with the moments for $r \leq q + 1$, while the diagonal elements have the information of the moments for $r \leq 2q + 1$. This could be imply the difference in the convergence properties of the bond energy and the forces. On a simple consideration it is estimated that the rate of the convergence of the force is about half as fast as that of the bond energy in terms of recursion levels. However it should be noted that the contribution of Θ_{0n}^L to Θ_{ij} decreases as the recursion level n increases, since the Lanczos vectors, which hop repeatedly in the atomic connectivity, have their weight away from the starting atom as the recursion level n increases. Thus, the bond-orders in the atomic basis representation do not have all the moments of the higher order more than the $(q + 1)$ th, but can include the higher moments through the \underline{G}_{0n}^L for $n < q$. In this case whereas the inexact moments for $r \leq 2q + 1 - n$ are included in the bond-order in the atomic basis representation, the error can be negligible, since the bond-orders Θ_{0n}^L become small as the recursion level n increases. So it is stressed that the higher moments can be included in the bond-order based on the atomic basis through the Green's function \underline{G}_{0n}^L for small recursion levels n . Therefore, it is expected that the forces should be comparable to the bond energy in terms of the convergence rate. In Sec. 2.2 we will discuss this point again numerically.

1.1.6 Details on implementation

The technical details to implement the block BOP are given here. For an infinite system, there could be an infinite number of levels in the multiple inverse of the diagonal Green's function. It is often the case, however, that the exact values can be replaced by estimated values after a certain number of levels, without reducing the accuracy significantly. The simplest approximation is to take $\underline{A}_n = \underline{A}_\infty$, $\underline{B}_n = \underline{B}_\infty$ for $n > n_t$, where n_t is the number of exact levels, and \underline{A}_∞ and \underline{B}_∞ are constant block elements. This approximation is reasonable from the observation that the scalar elements in both \underline{A}_n and \underline{B}_n converge to constant values or oscillate around constant values as n tends to infinity[37]. We have only to replace the level for $n = n_t + 1$ in the multiple inverse with the terminator, since the constant terms can be summed exactly. The terminator can be written by a closed form including itself as follows:

$$\underline{T}(Z) = [Z\underline{I} - \underline{A}_\infty - {}^t\underline{B}_\infty \underline{T}(Z) \underline{B}_\infty]^{-1}. \quad (1.73)$$

However, this is still a difficult set of equations to solve, so to simplify matters we assume that the off-diagonal elements of $\underline{T}(Z)$ are zero and all the diagonal elements are the same, since the differences between the diagonal elements of \underline{A}_n and \underline{B}_n become small as the number of the recursion levels increases, respectively. Then the identical diagonal element $t(Z)$ of $\underline{T}(Z)$ is written as the square root terminator:

$$t(Z) = [Z - a - b^2 t(Z)]^{-1}$$

$$= \frac{1}{b} \left[\frac{Z-a}{2b} - i\sqrt{1 - \left(\frac{Z-a}{2b}\right)^2} \right], \quad (1.74)$$

where a and b^2 are given by the means of the diagonal elements of \underline{A}_{nt} and \underline{B}_{nt}^2 , respectively. Thus, we see that the effect of the terminator is to smear out the sharp states with energy a into semielliptical bands. The degree of smearing is given by b .

There are two ways to conserve charge neutrality in the system: local charge neutrality (LCN)[10] or the total charge neutrality (TCN)[13]. Within LCN the on-site energies are varied (keeping the splitting between on-site s and p energy levels fixed) in order to conserve the number of electrons on each atom. If the excess charge on site i is $Q_i = Z_i - \sum_{\alpha} N_{i\alpha}$, where Z_i is the effective core charge, then the on-site energies can be shifted using the response function $X_i = \sum_{\alpha} X_{i\alpha}$ for atom i as follows:

$$\epsilon'_{i\alpha} = \epsilon_{i\alpha} - \lambda \frac{Q_i}{X_i}, \quad (1.75)$$

where λ is a parameter to accelerate the convergence, and generally is 1.0. The response function projected on an atomic orbital $i\alpha$ is given by

$$X_{i\alpha} = \frac{2}{\pi} \text{Im} \int [G_{i\alpha, i\alpha}(E + i0^+)]^2 f\left(\frac{E - \mu}{k_B T}\right) dE. \quad (1.76)$$

Usually no more than three or four iterations are required to achieve the convergence so that the absolute value of Q/atom is below 10^{-5} , since $X_{i\alpha} \simeq \partial N_{i\alpha} / \partial \epsilon_{i\alpha}$. The assumption of LCN has the advantage that the Madelung energy contribution is zero, so that the TB model needs not take this into account in its expression for the energy. Also LCN is suitable for parallel computation, since the calculations of the bond energy and the forces of each atom are perfectly independent within the assumption. However, LCN brings an inefficiency in terms of computational effort, since LCN requires the Lanczos algorithm to be implemented again, after the charge neutralities of all the atoms has been achieved, since the recursion block elements are varied by the shift of the on-site energies. Thus, the block Lanczos algorithm and the shift of the on-site energies must be repeated until self-consistency is accomplished. This self-consistency requires typically twenty iterations. This discourages us from applying LCN in the molecular dynamics simulations. On the other hand, we can conserve the total number of electrons in the system by a shift of the chemical potential in terms of TCN. If the excess charge of the system is $Q = \sum_i Q_i$, then a good approximation of the chemical potential is given by

$$\mu' = \mu + \lambda \frac{Q}{X}, \quad (1.77)$$

where $X = \sum_i X_i$. The convergence is achieved after only three or four iterations. The TCN assumption, corresponding to the micro canonical distribution, has physically appropriate meaning, which is consistent with the usual electronic structure calculations by diagonalization. Moreover within TCN we need not repeat the Lanczos algorithm, since the recursion block elements are not varied by the shift of the chemical potential. Thus, TCN has considerable advantage in terms of computational effort. The TCN condition reduces the separability of individual atoms in the calculations of the band energy and forces, and complicates

slightly the parallelizability of the program code. However, the evaluation and integration of the Green's function, which are time-consuming steps, are performed separately. Therefore, we use the TCN constraint to conserve the total number of electrons.

It is required to integrate the Green's functions with the Fermi function in order to evaluate the bond energy, bond-orders, and response functions. The integration can be carried out in the complex plane by summing up an infinite series over the modified Matsubara poles which is given in Appendix A[14, 15, 40]. The general form can be given as follows:

$$\text{Im} \int A(E + i0^+) f(x) dE = -\frac{2\pi}{\beta} \text{Re} \left[\lim_{P \rightarrow \infty} \sum_{p=0}^{P-1} z_p A(E_p) \right], \quad (1.78)$$

with

$$E_p = \mu + \frac{2P}{\beta} (z_p - 1), \quad z_p = \exp \left(\frac{i\pi(2p+1)}{2P} \right), \quad (1.79)$$

where $A(x)$ is an arbitrary function defined in the complex plane, and $\beta = 1/k_B T$. Also E_p are the poles of the approximated Fermi function in the complex plane. This modified Matsubara summation converges rapidly with about 40 complex poles ($P \simeq 40$) with a high electron temperature ($k_B T > 0.1 \text{ eV}$), although many poles are needed to achieve the convergence with a lower electron temperature. In the case of systems with a gap between the valence and conduction bands, we need to pay attention to the evaluation of the chemical potential, since the response functions in the gap become zero as $k_B T$ tends to 0, so that it is difficult to estimate the chemical potential under a low electron temperature using Eq. (1.75). This can be solved by smearing the density of states under a high electron temperature. Thus, it is required to evaluate the response functions at high electronic temperatures in order to obtain stable MD simulations.

We now estimate the time-dependence within the block BOP. The total system is divided into finite clusters centered on individual atoms in order to evaluate the energy and force of each atom. The size of the finite cluster is not determined by the size of the total system, but by the system and the condition of the MD simulation. Therefore, the computational effort is proportional to the number of atoms N_{atom} , so that the number of computational operations can be written as cN_{atom} , where c is a proportionality constant. The scaling of the constant c can be estimated as a function of the numbers of recursion level q , atoms within a finite cluster n_c , and orbitals on an atom M . For simplicity it is assumed that the system consists of only one type of element with M orbitals. In the block Lanczos algorithm the time-consuming step is the product of the Hamiltonian matrix by the vector, so that the count of operations in the block Lanczos algorithm is nearly proportional to $qn_c^2 M$. At the next step, the inverses and recursive calculations are required to evaluate the diagonal and off-diagonal elements of the Green's function matrix, respectively, and their integrations are performed as the sum of the residues for the poles in the complex plane, so that the count of operations for the evaluations is almost proportional to qPM^3 . Thus, the proportionality constant c can be estimated as $c_L \times qn_c^2 M + c_G \times qPM^3$, where c_L and c_G are prefactors of the count of operations for the block Lanczos algorithm and the the evaluation of the bond-orders, respectively. The prefactors depend on the computer, and the system, and the criterion of charge neutrality. For example, for the case of a 3 hop cluster, 10 recursion

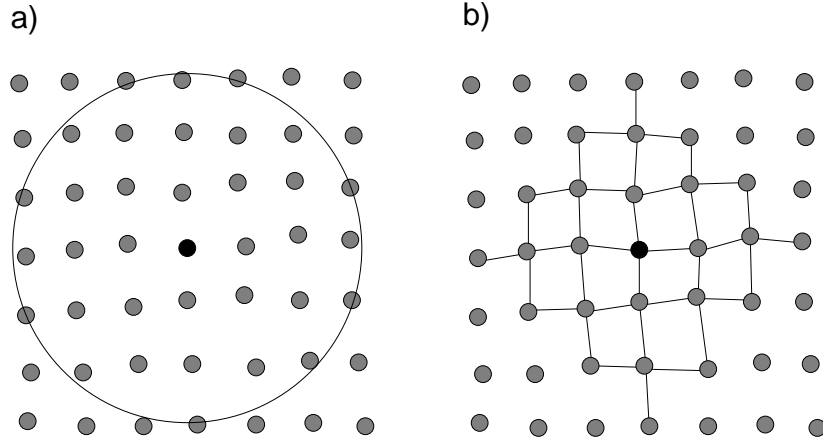


Figure 1.2: The physically (a) and logically (b) truncated clusters in a infinite disordered square lattice. The physical truncation determines the cluster by selecting atoms within a given radius of a sphere centered an atom. On the other hand, the logical truncation constructs the cluster from the connectivity of the bondings, where we regard a pair of two atoms forms the bonding when the distance of two atoms is smaller than a given length.

levels, and 40 complex poles for diamond carbon, the calculation time of the block Lanczos algorithm is comparable to that in evaluating and integrating the Green's functions.

In the remainder of this subsection the procedure for implementing the block BOP is enumerated. (I). The partition of the system. The hopping range of each atom is determined by terminating the system. There are two ways to terminate the system as shown in Fig. 1.2. One of them is the physical truncation that the terminated cluster contains atoms within a sphere with a certain cutoff radius. The physical truncation can bring inaccurate properties into the convergence of the energies, since atoms that have no bonding to other atoms can be included in the neighborhood of the cluster surface. Moreover, in MD simulations the energies can jump discontinuously when an atom moves in or out of the surface of the sphere. The more stable way is logical truncation. The cluster of size n is here defined by all neighbors that can be reached by n hops. Provided the cutoff distance for the hopping integral is identical to that defining the connectivity of the bonding, the energies are continuous as a function of time in MD simulations. Therefore, it is desirable to truncate logically the system in terms of accuracy. (II). The block Lanczos algorithm. The Hamiltonians for the individual terminated clusters are constructed. For these small cluster Hamiltonians the block Lanczos algorithm Eqs. (1.38)~(1.45) is applied. (III). The evaluations and integrations of the Green's functions. In the Lanczos basis representation the diagonal and the off-diagonal elements of the Green's functions are evaluated using Eqs. (1.56) and (1.57), respectively, and then their integrations are performed via the modified Matsubara summation with Eq. (1.78). (IV). The transformation into the atomic basis representation. The bond-orders based on the Lanczos basis are transformed into those in the atomic basis representation using Eq. (1.52). (V). The bond energy and forces. From Eqs. (1.3) and (1.9) the bond energy and forces are evaluated, respectively.

1.1.7 Analytic example

Let us apply the method to the s -valent Bethe lattice which branches at each lattice point in K -fold as an analytic example of the block BOP. It is assumed that each on-site energy is $\epsilon (\leq 0)$, a hopping integral between the nearest neighbor atoms is $-h$ ($0 < h$), and the other hopping integrals are zero. The number of n -th neighbor atoms, which can be reached in the process of n -hopping from a central atom, for a central atom in the K -fold Bethe lattice is given by $C_n = K(K-1)^{n-1}$ for $n \geq 1$, and the total number of atoms which participate in the process of the n -hopping is written as $S_n = (K(K-1)^n - 2)/(K-2)$ for $n \geq 0$. Therefore, starting the recursion with a central atom as the starting state in the Lanczos algorithm, we can write the Lanczos bases as follows:

$$\langle L_0 | = (1, 0, 0, \dots,). \quad (1.80)$$

$$\langle L_n | = \frac{1}{\sqrt{K(K-1)^{n-1}}} (\overbrace{0, \dots, 0}^{S_n - C_n}, \overbrace{1, \dots, 1}^{C_n}, 0, 0, \dots,) \quad \text{for } n \geq 1. \quad (1.81)$$

From Eq. (1.81) we see that the Lanczos bases in the s -valent Bethe lattice are reflected only the spreading process of an electron, since the recoil process is omitted in the developed vectors through the orthonormalization in the Lanczos algorithm. By using the Lanczos bases, the recursion chain coefficients A_n and B_n , which correspond on-site energies and hopping integrals in the transformed semi-infinite chain cluster, respectively, are given by

$$A_n = \langle L_n | \hat{H} | L_n \rangle = \epsilon. \quad (1.82)$$

$$B_n = \langle L_n | \hat{H} | L_{n-1} \rangle = \begin{cases} -\sqrt{K} h, & \text{for } n = 1, \\ -\sqrt{K-1} h, & \text{for } n \geq 2. \end{cases} \quad (1.83)$$

B_n for $n = 1$ is different from that for $n \geq 1$ since the number of virgin sites which can be hopped from the central atom is one more than that of the other sites. Considering that the recursion chain coefficients are elements of the tridiagonalized Hamiltonian, then the off-diagonal Green's function may be written explicitly as a continued fraction:

$$G_{00}^L(Z) = \frac{1}{Z - \epsilon - \frac{Kh^2}{Z - \epsilon - \frac{(K-1)h^2}{Z - \epsilon - \frac{(K-1)h^2}{Z - \epsilon - \dots}}}} \quad (1.84)$$

The continued fraction expressed in self-similar form can be compactly rewritten by using a square root terminator as follows:

$$G_{00}^L(Z) = \frac{1}{\left(1 - \frac{K}{2(K-1)}\right) (Z - \epsilon) + \frac{K}{2(K-1)} \sqrt{(Z - \epsilon)^2 - 4(K-1)h^2}}. \quad (1.85)$$

In the off-diagonal Green's functions based on the Lanczos basis, only $G_{01}^L(Z)$ which is defined between the starting site and the first Lanczos vector is required in order to calculate

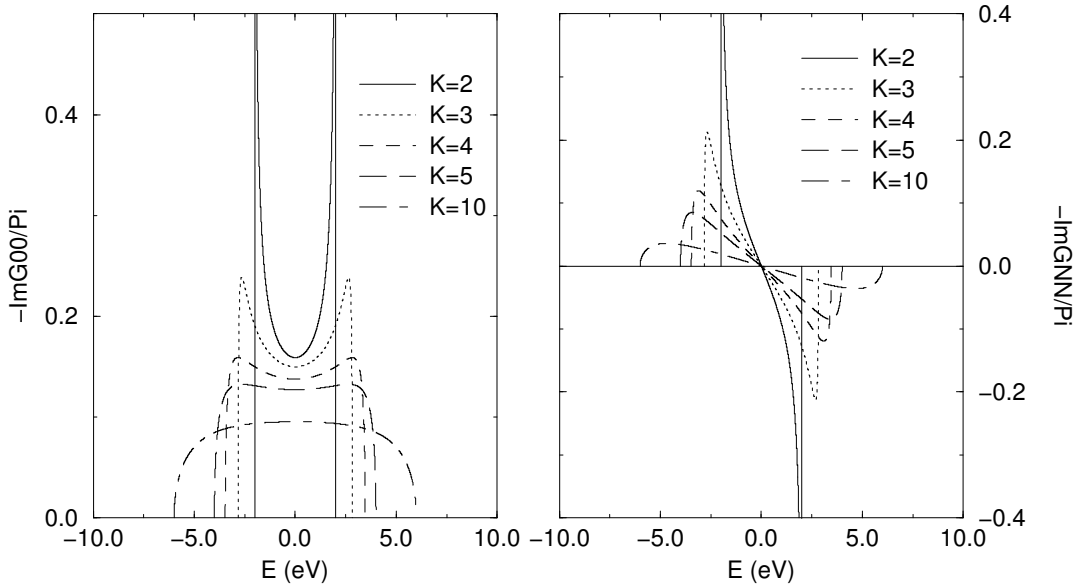


Figure 1.3: The imaginary parts of the diagonal (left panel) and the nearest neighbor off-diagonal (right panel) Green's functions on the s-valent Bethe lattice for $K = 2, 3, 4, 5,$ and 10 , where $\epsilon = 0$ and $h = 1$ eV.

the bond-order between the nearest neighbor atoms, since the contribution of the nearest neighbor atoms for the central atom appears only the first Lanczos vector. The Green's function $G_{01}^L(Z)$ is calculated by the recurrence relation Eq. (1.57), and then $G_{01}^L(Z)$ the based on the Lanczos basis is transformed into that of the atomic basis representation. Thus, the Green's function $G_{NN}(Z)$ between the nearest neighbor atoms is given by

$$G_{NN}(Z) = -\frac{1}{Kh} \left\{ G_{00}^L(Z)(Z - \epsilon) - 1 \right\}. \quad (1.86)$$

In Fig. (1.3) we show the imaginary parts of Eqs. (1.85) and (1.86). While the local density of states of $K = 2$ has clearly singularities of Van-Hove which characterize an one-dimensional lattice, the singularities in the local density of states become indistinct with increasing number of coordinates K . Also the width of the band is $4|h|\sqrt{K-1}$. The imaginary parts of the off-diagonal Green's functions show that from the bottom of the band until the center corresponds to the bonding states, on the other hand, the band above the center comes from the anti-bonding states. The increase of K reduces the bond-order between the nearest neighbor atoms with the relation of the approximately inverse proportional ratio.

When $K = 2$ corresponding to a chain which is the simplest Bethe lattice, we can easily carry out analytic integrals of G_{00}^L and G_{01}^L . If it is assumed that the total number of electrons is equivalent to that of sites, then the number of electrons on each site is $N = 1$, and the bond-order between the nearest neighbor atoms is given as $\Theta_{NN} = 2/\pi \simeq 0.6366$. Next we shall compare the exact bond-order with those at the first, second, and third levels in the Lanczos algorithm. Approximating the exact Green's function at the first, second, third, and fourth levels in the continued fraction, we can write the off-diagonal Green's functions

between the nearest neighbor sites, respectively, as follows:

$$G_{NN}^{\text{First}}(Z) = \frac{\frac{\sqrt{2}}{4}}{Z + \sqrt{2} h} + \frac{-\frac{\sqrt{2}}{4}}{Z - \sqrt{2} h}, \quad (1.87)$$

$$G_{NN}^{\text{Second}}(Z) = \frac{\frac{\sqrt{3}}{6}}{Z + \sqrt{3} h} + \frac{-\frac{\sqrt{3}}{6}}{Z - \sqrt{3} h}, \quad (1.88)$$

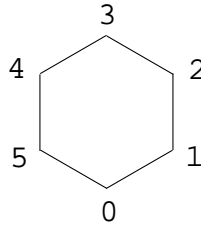
$$G_{NN}^{\text{Third}}(Z) = \frac{\frac{\sqrt{2+\sqrt{2}}}{8}}{Z + \sqrt{2 + \sqrt{2}} h} + \frac{\frac{\sqrt{2-\sqrt{2}}}{8}}{Z + \sqrt{2 - \sqrt{2}} h} + \frac{\frac{-\sqrt{2+\sqrt{2}}}{8}}{Z - \sqrt{2 + \sqrt{2}} h} + \frac{\frac{-\sqrt{2-\sqrt{2}}}{8}}{Z - \sqrt{2 - \sqrt{2}} h}, \quad (1.89)$$

$$G_{NN}^{\text{Fourth}}(Z) = \frac{\frac{1}{10} \sqrt{\frac{5+\sqrt{5}}{2}}}{Z + \sqrt{\frac{5+\sqrt{5}}{2}} h} + \frac{\frac{1}{10} \sqrt{\frac{5-\sqrt{5}}{2}}}{Z + \sqrt{\frac{5-\sqrt{5}}{2}} h} + \frac{\frac{-1}{10} \sqrt{\frac{5+\sqrt{5}}{2}}}{Z - \sqrt{\frac{5+\sqrt{5}}{2}} h} + \frac{\frac{-1}{10} \sqrt{\frac{5-\sqrt{5}}{2}}}{Z - \sqrt{\frac{5-\sqrt{5}}{2}} h}, \quad (1.90)$$

where constant terms were omitted, since they have no contribution to the bond-order. Considering the residues of the states which are occupied in these Green's functions, we see that the approximated bond-order are 0.7071, 0.5774, 0.6533, and 0.6155 at the first, second, third, and fourth levels, respectively, and also the errors of these approximated bond-orders are 11.1, -9.3, 2.6, and -3.3 %, respectively, compared with the exact value 0.6366. Thus, the analytic example shows that the bond-order can be reproduced with a considerable accuracy at a few finite level of approximations even the sparse structure such as the linear chain which has singularities in the density of states.

Additional derivation (D)

A simple analytic example is given, which is helpful to understand the recursion method. Let us consider π electron of a benzene molecule described by the Huckel theory.



$$H = \begin{pmatrix} a & b & 0 & 0 & 0 & b \\ b & a & b & 0 & 0 & 0 \\ 0 & b & a & b & 0 & 0 \\ 0 & 0 & b & a & b & 0 \\ 0 & 0 & 0 & b & a & b \\ b & 0 & 0 & 0 & b & a \end{pmatrix}$$

Lanczos process:

(1)

$$|u_0 \rangle = (1, 0, 0, 0, 0, 0)^t$$

(2)

$$H|u_0 \rangle = (a, b, 0, 0, 0, b)^t$$

(3)

$$\alpha_0 = \langle u_0 | H | u_0 \rangle = a$$

(4)

$$\begin{aligned} |r_0 \rangle &= H|u_0 \rangle - \alpha_0|u_0 \rangle \\ &= (0, b, 0, 0, 0, b)^t \end{aligned}$$

(5)

$$\begin{aligned} \beta_1^2 &= \langle r_0 | r_0 \rangle \\ &= 2b^2 \\ \beta_1 &= \sqrt{2}b \end{aligned}$$

(6)

$$\begin{aligned} |u_1 \rangle &= \frac{1}{\beta_1} |r_0 \rangle \\ &= \frac{1}{\sqrt{2}} (0, 1, 0, 0, 0, 1)^t \end{aligned}$$

(7)

$$H|u_1 \rangle = \frac{1}{\sqrt{2}} (2b, a, b, 0, b, a)^t$$

(8)

$$\alpha_1 = \langle u_1 | H | u_1 \rangle = a$$

(9)

$$\begin{aligned}
|r_1 \rangle &= H|u_1 \rangle - \beta_1|u_0 \rangle - \alpha_1|u_1 \rangle \\
&= \frac{1}{\sqrt{2}}(0, 0, b, 0, b, 0)^t
\end{aligned}$$

(10)

$$\begin{aligned}
\beta_2^2 &= \langle r_1|r_1 \rangle \\
&= b^2 \\
\beta_2 &= b
\end{aligned}$$

(11)

$$\begin{aligned}
|u_2 \rangle &= \frac{1}{\beta_2}|r_1 \rangle \\
&= \frac{1}{\sqrt{2}}(0, 0, 1, 0, 1, 0)^t
\end{aligned}$$

(12)

$$H|u_2 \rangle = \frac{1}{\sqrt{2}}(0, b, a, 2b, a, b)^t$$

(13)

$$\alpha_2 = \langle u_2|H|u_2 \rangle = a$$

(14)

$$\begin{aligned}
|r_2 \rangle &= H|u_2 \rangle - \beta_2|u_1 \rangle - \alpha_2|u_2 \rangle \\
&= \frac{1}{\sqrt{2}}(0, 0, 0, 2b, 0, 0)^t
\end{aligned}$$

(15)

$$\begin{aligned}
\beta_3^2 &= \langle r_2|r_2 \rangle \\
&= 2b^2 \\
\beta_3 &= \sqrt{2}b
\end{aligned}$$

(16)

$$\begin{aligned}
|u_3 \rangle &= \frac{1}{\beta_3}|r_2 \rangle \\
&= (0, 0, 0, 1, 0, 0)^t
\end{aligned}$$

(17)

$$H|u_3 \rangle = (0, 0, b, a, b, 0)^t$$

(18)

$$\alpha_3 = \langle u_3|H|u_3 \rangle = a$$

(19)

$$\begin{aligned} |r_3\rangle &= H|u_3\rangle - \beta_3|u_2\rangle - \alpha_3|u_3\rangle \\ &= (0, 0, 0, 0, 0, 0)^t \end{aligned}$$

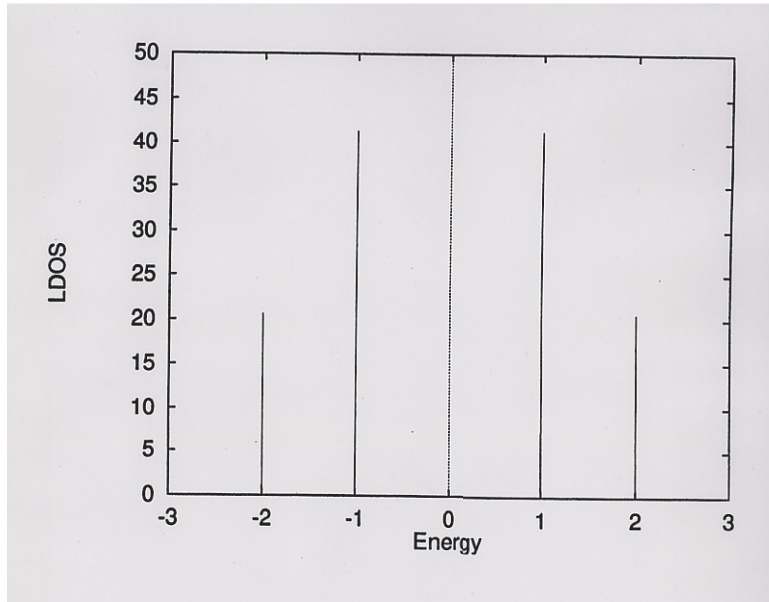
So, we have a tridiagonalized Hamiltonian:

$$H_{\text{TD}} = \begin{pmatrix} a & \sqrt{2}b & 0 & 0 \\ \sqrt{2}b & a & b & 0 \\ 0 & b & a & \sqrt{2}b \\ 0 & 0 & \sqrt{2}b & a \end{pmatrix}$$

Green's functions can be written as follows:

$$G_{00}^{TD}(Z) = \frac{1}{Z - a - \frac{2b^2}{Z - a - \frac{b^2}{Z - a - \frac{2b^2}{Z - a}}}}$$

Let Z be $E + i\varepsilon$, and us write the outline of $\text{Im}G_{00}^{TD}$ where $\varepsilon = 10^{-5}$, $a = 0$, and $b = -1$, so we see the local density of states for π electron of a benzene:



1.2 Convergence Properties

$O(N)$ methods with linear scaling algorithms are approximate approaches compared to the exact diagonalization for dealing with large scale systems, so that the realization of the $O(N)$ algorithms is accompanied by decreases in computational accuracy in exchange for computational efficiency. Therefore, $O(N)$ methods should only be applied to atomistic simulations once their accuracy and efficiency has been tested.

In the block BOP three approximations are introduced to reduce the computational effort: the number of moments, or recursion levels, the size of the cluster of atoms over which the hops are made, and a finite number of poles in the modified Matsubara summation which gives accurately integration of Green's functions with the Fermi function within a small number of poles. The finite approximations for the number of levels and the size of the cluster can lead to the errors in the energies and forces. Thus, we now investigate the block BOP through several test calculations in terms of its accuracy and efficiency. In order to ascertain applicable bounds for a wide range of materials, the energy and force convergence are examined for an insulator (carbon[41] in the diamond structure), a semiconductor (silicon[42]), a metal (titanium, described by a canonical d-band model), and a molecule (benzene[43]) as functions of the number of recursion levels and the size of cluster. In all the test calculations, we have chosen the same value (40 poles) as the number of poles in the modified Matsubara summation. The 40 poles is enough to achieve convergence in carbon, silicon, titanium, and benzene materials in case of $k_B T = 0.1$ eV used in all the numerical tests[15]. Moreover, in terms of the computational efficiency the block BOP is compared with k-space calculations in computational time. Also as a test of the quality of the forces, we perform a constant energy molecular dynamics (CEMD) simulation of carbon.

1.2.1 Energy convergence

Figure 2.4 shows the cohesive energy per atom for carbon in the diamond structure, silicon in the diamond structure, hcp titanium, and benzene. The cohesive energies were calculated using 2 ~ 15 recursion levels (a numerical instability often appears for > 20 recursion levels) for three, five, and seven shell clusters by the logical truncation method, where the three, five, and seven shell clusters for the diamond structure include 41, 147, and 363 atoms, respectively, and these clusters for the hcp structure contain 153, 587, and 1483 atoms, respectively. The cohesive energies for carbon and silicon converge rapidly to the results of k-space calculations. The errors for carbon and silicon are only 1 % at six recursion levels. Thus, we see that up to the 13th moment corresponding to six recursion levels determine the cohesive energies. The contribution of the higher order moments is unimportant, since the convergence properties are almost identical for three, five, and seven shell clusters. The cohesive energy for silicon converges more slowly compared with that of carbon in the rate of convergence for the size of cluster. This suggests that a semiconductor such as silicon requires higher moment than an insulator such as carbon for good convergence of the cohesive energy.

The cohesive energy for the metallic hcp titanium converges very quickly in terms of the number of recursion levels. For the five and seven shell clusters the cohesive energy converges fully to the k-space result, while the convergence value for the three shell cluster is in error by 2 % from the k-space result. For benzene the convergence is achieved with a very small cluster (2 shells). The error at four recursion levels is only 0.1%. We see that the block BOP can evaluate accurately the cohesive energy for a molecule with a sparse structure like benzene, which has both localized σ bonds and delocalized π bonds.

The calculation of the vacancy formation energy is a severe test to distinguish the accuracy of different $O(N)$ methods, since it is a criterion that tests the precision which the dangling bonds caused by the vacancy are handled by $O(N)$ method. In practice, the usual moment-based $O(N)$ methods fail to reproduce the vacancy formation energy of carbon in

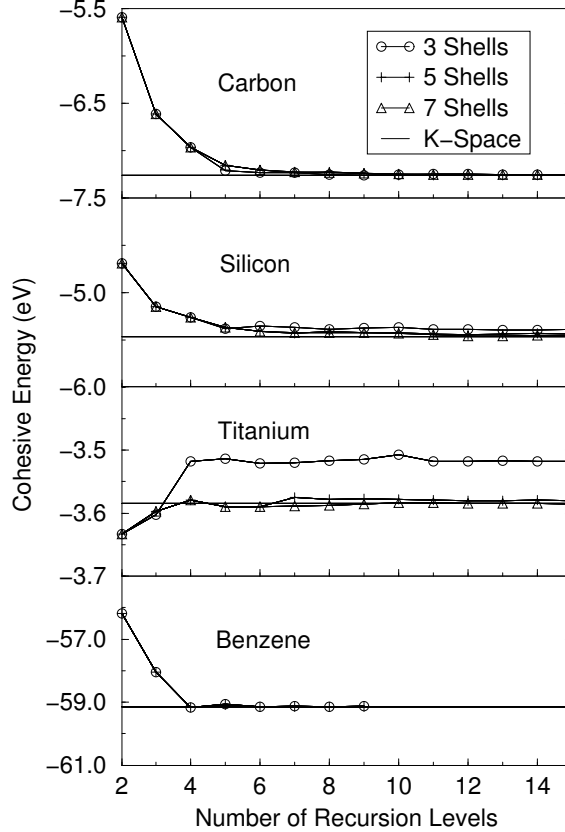


Figure 1.4: The cohesive energy for carbon in the diamond structure, silicon in the diamond structure, hcp titanium, and benzene as a function of number of recursion levels for three, five, and seven shell clusters, calculated using a square root terminator, a total charge neutrality, and $k_B T = 0.1$ eV.

the diamond structure even when dozens of moments are included[27, 28]. The computational error at 30 moments is still about 20 % compared to the k-space result. In Fig. 1.5 we show the vacancy formation energy for carbon in the diamond structure, silicon in the diamond structure, and hcp titanium. These are calculated as the difference between the energy for a bulk unit cell (of 64, 64 or 32 atoms, respectively) with a single atom removed, and the perfect bulk cell energy scaled to 63, or 31 atoms. The results are for an unrelaxed vacancy. The convergence properties for carbon and silicon are almost identical. The vacancy formation energy in the five and seven shell clusters converges smoothly toward the k-space results, while in the 3 shell cluster the converged values for carbon and silicon are 15 %, and 13 % underestimated, respectively. In the seven shell cluster at 15 recursion levels the errors for carbon and silicon are only 1%. Thus, we see that the block BOP gives an accurate vacancy formation energy for strongly covalent materials such as carbon and silicon with the use of about 30 block moments. This remarkable result suggests that the block BOP accurately describes dangling bonds in comparison with the usual moment-based methods. For titanium the vacancy formation energy converges to the k-space result equally within the three, five, and seven shell clusters. The error for the 3 shell cluster at 5 recursion levels is about 6%. The vacancy formation energy oscillates with respect to the number

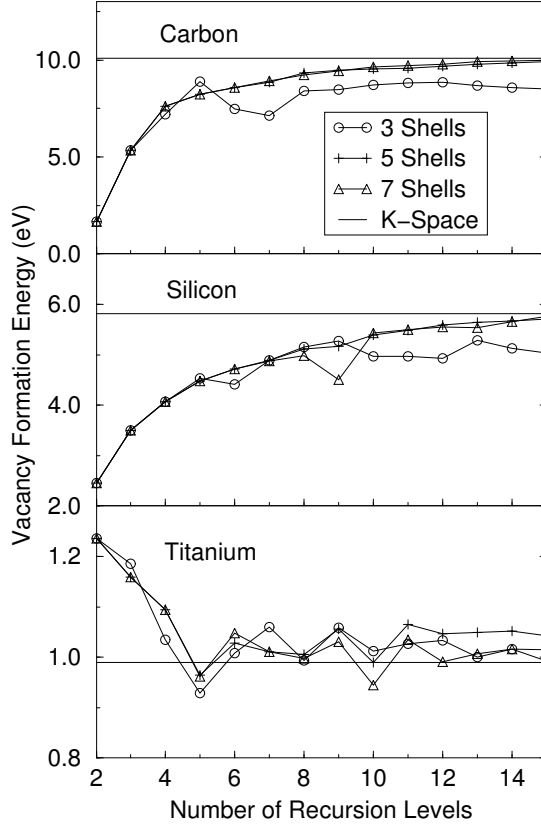


Figure 1.5: The vacancy formation energy for carbon in the diamond structure, silicon in the diamond structure, and hcp titanium for three, five, and seven shell clusters as a function of number of recursion levels, calculated using a square root terminator, a total charge neutrality, and $k_B T = 0.1$ eV.

of recursion levels due to the long range value of the density matrix (see fig. 2 of ref. 23). The oscillations are damped by imposing LCN instead of TCN to conserve the number of electrons.

1.2.2 Force convergence

The accuracy of the forces is investigated from two different perspectives. The first is the accuracy when compared to the exact k-space result, the second is the degree of correspondence between the numerical and analytic Hellmann-Feynman forces. In order to perform reliable MD simulations the two criteria should be satisfied. In Fig. 1.6 we show the z -component of the force on an atom in the bulk-terminated (001) surface of carbon, silicon, and hcp titanium, and the force on a hydrogen atom on benzene. For carbon the force of the three shell cluster overestimates by about 130 % in comparison with the k-space result, although the error in the Hellmann-Feynman term is only 1 %. The forces of the five and seven shell clusters converge smoothly toward the k-space result. The rate of convergence in silicon is much better than that of carbon. Even the three shell cluster shows a converged value that differs by only 5 % from the k-space result. The three, five, and seven shell clusters of Ti show similar convergence properties of the forces, the converged value being underestimated

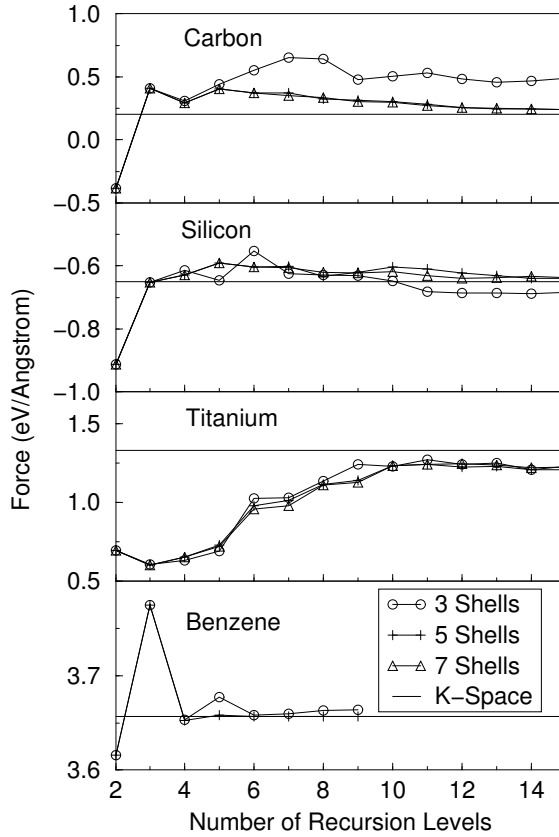


Figure 1.6: The z -component of the force on an atom on the carbon (001) surface, silicon (001) surface, titanium (001) surface, and on a hydrogen atom in benzene for three, five, and seven shell clusters as a function of number of recursion levels, calculated using a square root terminator, total charge neutrality, and $k_B T = 0.1$ eV.

by about 8% compared with the k-space result. For benzene the force converges rapidly with small cluster size. As discussed in Sec. 1.1.5 the bond-orders can be expanded using the lower order moments compared with the density of states in the block BOP. It can be estimated that the forces should converge more slowly at the k-space results than the bond energies, since the forces on the atoms are evaluated using the bond-orders. However, these numerical results for the forces show that the convergence rate of the force is comparable to that of the bond energy. This means that the sum of Eq. (1.52) converges rapidly as the number of the recursion levels increases because of the diffusion of the Lanczos vectors.

As a test of the consistency between the total energy and the forces, constant energy molecular dynamics (CEMD) simulations have been performed for carbon. If the forces are equal to the derivative of the total energy with respect to atomic positions, the total energy of the system is conserved. Thus, the CEMD simulation is a criterion to investigate the consistency of forces. In Fig. 1.7 we show the energy for carbon at 1000 and 5000 K as a function of time using five and ten recursion levels. The initial structure is the diamond lattice, and the unit cell is fixed in volume and shape. When the initial temperature of the system is 1000 K, the atoms oscillate around the equilibrium positions. At five and ten recursion levels we see that the total energy is almost conserved. When the temperature

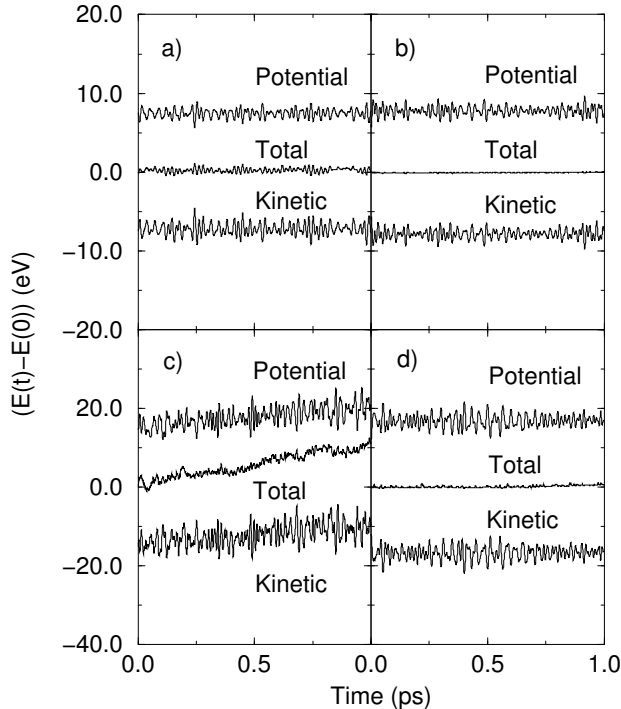


Figure 1.7: The potential, kinetic, and total energies as a function of time for molecular dynamics simulations of carbon using a three hop logically truncated cluster, a square root terminator, total charge neutrality, and $k_B T = 0.1$ eV. In panels (a) and (b) the results are for five and ten recursion levels at 1000 K, respectively, whereas in panels (c) and (d) they are for five and ten recursion levels at 5000 K, respectively. The time step is 0.5 fs.

is raised to 5000 K, the carbon in the diamond structure transforms into liquid carbon with mainly three coordinate structure. From Fig. 1.7 we see that the forces are of good quality at ten recursion levels, while the total energy at five recursion levels increases by about 10 eV during the 1 ps, which corresponds to a temperature increase of 1800 K. These results indicate that the block BOP can give forces consistent with the total energy, provided the proper number of recursion levels is used, even for liquid materials such as carbon at a high temperature. On the other hand, in the variational DM method, although only the Hellmann-Feynman term survives formally as the derivatives of the band energy with respect to atomic coordinates, total energy of liquid silicon in the CEMD simulation exhibits a steady upward drift[44].

1.2.3 Computational efficiency

To study the computational efficiency of the block BOP we carry out two benchmark tests: the comparison between the block BOP and the k-space calculation in computer time, and the relation between the computational error and the computer time. Figure 1.8 shows the time to evaluate the energy and forces for a cell containing carbon in the diamond structure as function of the number of atoms in the cell for the block BOP and k-space using a single k-point. The crossover point at which the block BOP becomes favorable is about 100 atoms.

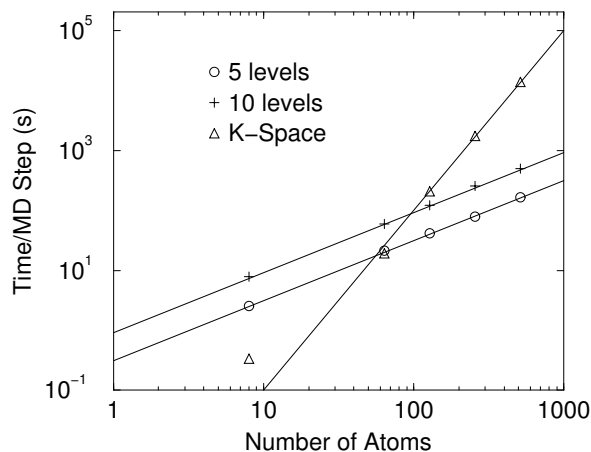


Figure 1.8: The time to perform the energy and the force evaluation for carbon in the diamond structure as a function of number of atoms in the cell for the block BOP, calculated using a three hop logically truncated cluster, and k-space. The calculations were performed on an IBM RS/6000 workstation.

Figures 1.9(a) and (b) show the relation between the error and the the time per atom to evaluate the energy and forces in the calculations of the vacancy formation energy of diamond carbon and hcp titanium, respectively. Here the increase in time corresponds to the increase of the number of recursion levels. We see that the block BOP can calculate the vacancy formation energy to high accuracy within almost the same computational time as the other moment-based results reported by Bowler et al.[27] where the calculations were performed using the same computational facilities. We note that the block BOP has given a good convergent result of the vacancy formation energy in diamond carbon for the first time with a moments-based method, while the computational time to achieve this convergence is still ten times slower than that of the DM method. This work, therefore, still supports the conclusions of the study in ref. 23 that the DMM is best for systems with energy gaps, but that moments-based methods such as BOP are best for metallic systems.

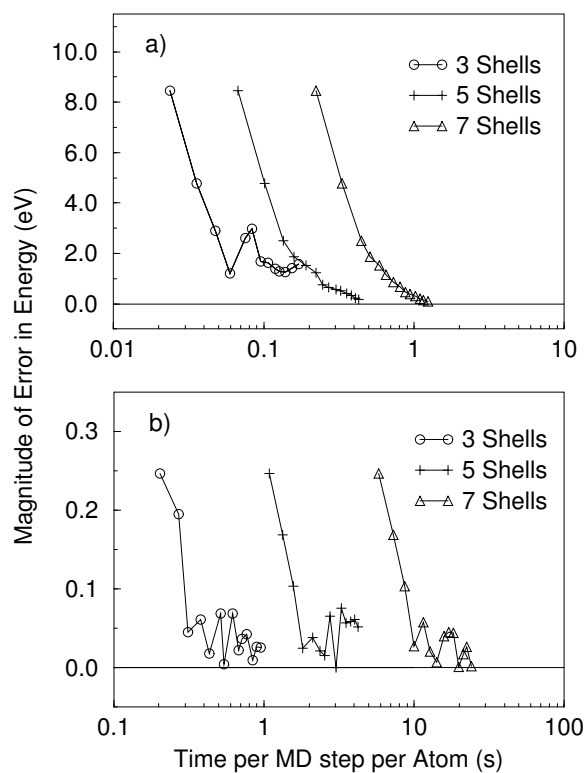


Figure 1.9: The error in the carbon (a) and titanium (b) vacancy formation energies against the time taken per MD step per atom for three, five, and seven shell clusters. The calculations were carried out with a square root terminator, total charge neutrality, and $k_B T = 0.1$ eV on a HP9000/735 workstation.

Chapter 2

Non-Orthogonal Basis Sets

In this chapter, the generalization of recursion methods to non-orthogonal basis orbitals are discussed, which is a crucial step to make the recursion method applicable to *ab initio* electronic structure calculations such as density functional theories and Hartree-Fock methods.

2.1 Non-orthogonal basis sets

In the non-orthogonal basis set, the overlap matrix is defined by

$$S_{i\alpha,j\beta} = \langle i\alpha | j\beta \rangle. \quad (2.1)$$

An orthogonality relation similar to that of the orthogonal case can be obtained by introducing the dual basis defined by

$$|i\tilde{\alpha}\rangle = \sum_{j\beta} S_{i\alpha,j\beta}^{-1} |j\beta\rangle, \quad (2.2)$$

where S^{-1} is the inverse of the overlap matrix S . It is then easy to verify that

$$\langle i\tilde{\alpha} | j\beta \rangle = \delta_{i\alpha,j\beta}. \quad (2.3)$$

A similar complete relation can be also given in a mixed form of the non-orthogonal basis and the dual basis as follows:

$$\sum_{i\alpha} |i\tilde{\alpha}\rangle \langle i\alpha| = \sum_{i\alpha} |i\alpha\rangle \langle i\tilde{\alpha}| = 1. \quad (2.4)$$

By using the overlap matrix Eq. (2.1), the secular equation based on the non-orthogonal basis set can be written in the DFT as follows:

$$HC = SCE, \quad (2.5)$$

where the C -matrix is defined by expansion coefficients $C_{i\alpha,\phi} = \langle i\tilde{\alpha} | \phi \rangle$ of one-particle eigen functions $|\phi\rangle$ based on the non-orthogonal basis, and the diagonal elements of the diagonalized E -matrix are the eigen values corresponding to the one-particle eigen functions. The one-particle eigen functions derived from Eq. (2.5) form a set of orthonormal functions. Thus, the orthonormality can be expressed in matrix form as follows:

$${}^\dagger CSC = I. \quad (2.6)$$

The traces of both sides in Eq. (2.6) provide the total number of electrons in a system:

$$N_{\text{ele}} = \sum_{ij} \text{tr} \left\{ \underline{\Theta}_{ij} \underline{S}_{ji} \right\}. \quad (2.7)$$

The summation of only an atom i or j gives the atomic population defined by Mulliken[?]. Moreover, taking into account both Eqs. (2.5) and (2.6), we get an expression which gives the band energy in terms of the bond-order similar to that of the orthogonal basis set as follows:

$$\begin{aligned} E_{\text{band}} &= 2 \text{tr} \{E\} \\ &= 2 \text{tr} \left\{ {}^\dagger C H C \right\} \\ &= \sum_{ij} \text{tr} \left\{ \underline{\Theta}_{ij} \underline{H}_{ji} \right\}. \end{aligned} \quad (2.8)$$

In comparison with Eq. (2.3) we see that the band energy in the non-orthogonal basis set is given by the identical expression which is derived in the orthogonal basis set. In contrast to the similarity, the force expression in the non-orthogonal basis set includes the correction term which comes from the derivatives of the expansion coefficients in addition to the Hellmann-Feynman term. Differentiating Eqs. (2.8) with respect to the atomic coordinates, substituting Eq. (2.6) and the derivative of Eq. (2.8) for the corresponding terms in the derivative of Eqs. (2.8), we get

$$\begin{aligned} F_k^{(\text{band})} &= -2 \text{tr} \left\{ {}^\dagger C \frac{\partial H}{\partial \mathbf{r}_k} C \right\} + 2 \text{tr} \left\{ {}^\dagger C \frac{\partial S}{\partial \mathbf{r}_k} C E \right\} \\ &= -\sum_{ij} \text{tr} \left\{ \underline{\Theta}_{ij} \frac{\partial \underline{H}_{ji}}{\partial \mathbf{r}_k} \right\} + \sum_{ij} \text{tr} \left\{ \underline{\Lambda}_{ij} \frac{\partial \underline{S}_{ji}}{\partial \mathbf{r}_k} \right\} \end{aligned} \quad (2.9)$$

with

$$\underline{\Lambda}_{ij} = -\frac{2}{\pi} \text{Im} \int E \underline{G}_{ij}(E + i0^+) f(x) dE, \quad (2.10)$$

where the second term in Eq. (2.9) gives the correction to the Hellmann-Feynman force in the non-orthogonal basis set. It is appropriate in terms of the computational efficiency that the correction term excludes the derivatives of the expansion coefficients. Hence in order to evaluate the band energy and the derivatives in the non-orthogonal basis set, we need to calculate the diagonal and the off-diagonal Green's functions as well as the orthogonal basis set. In following description, we discuss four three generalized recursion methods in order to develop an accurate, efficient, and robust $O(N)$ method.

2.2 Algorithm A

2.2.1 Formalism

In the non-orthogonal basis the one particle Green's function operator $\hat{G}(Z)$ has to satisfy the same identity $\hat{G}(Z)(Z - \hat{H}) = \hat{1}$ in comparison to the orthogonal case. Inserting the complete relation Eq. (2.4) into the identity, and operating $\langle i\tilde{\alpha}|$ and $|i\alpha\rangle$ from the left and

the right sides, respectively, we see that the Green's function matrix based on the dual basis can be obtained by the inverse of $(ZS - H)$ based on the original non-orthogonal basis. Then, the Green's function matrix based on the dual basis can be simplified by inserting the orthogonality Eq. (2.6) as follows:

$$\begin{aligned} G^D(Z) &= (ZS - H)^{-1} \\ &= [SC(ZI - {}^\dagger CHC)^\dagger CS]^{-1} \\ &= C(ZI - E)^{-1} {}^\dagger C, \end{aligned} \quad (2.11)$$

where the index D of the Green's function represents the dual basis representation. Therefore, we see that the element of the Green's function matrix provides the bond-order based on the non-orthogonal basis in similar form compared that in the orthogonal case.

Next we extend the block Lanczos algorithm into the non-orthogonal case. The basic idea for extending to the non-orthogonal case is only to find a matrix U which diagonalizes the overlap and block-tridiagonalize the Hamiltonian matrices simultaneously. That is,

$${}^\dagger USU = I, \quad (2.12)$$

$${}^\dagger UHU = H_{\text{BTD}}, \quad (2.13)$$

where H_{BTD} means the block-tridiagonalized Hamiltonian which is equivalent to H^L based on the Lanczos basis as shown later on. Multiplying U by both sides of Eq. (2.13), and substituting $U^\dagger US = I$, we have

$$H'U = UH_{\text{BTD}}, \quad (2.14)$$

where the modified Hamiltonian H which is not any more hermitian is given by $H' = S^{-1}H$. Regarding Eq. (2.14) as a scattering equation for an electron, and solving conversely it, we can write a series of procedures for the block Lanczos algorithm in the non-orthogonal case as follows:

$$|U_0\rangle = (|i1\rangle, |i2\rangle, \dots, |iM_i\rangle). \quad (2.15)$$

$$\underline{A}_n = (U_n | \hat{H} | U_n). \quad (2.16)$$

$$|r_n\rangle = \hat{H}'|U_n\rangle - |U_{n-1}\rangle {}^t \underline{B}_n - |U_n\rangle \underline{A}_n. \quad (2.17)$$

$$(\underline{B}_{n+1})^2 = (r_n | \hat{S} | r_n). \quad (2.18)$$

$$(\lambda_n)^2 = {}^t \underline{V}_n (\underline{B}_{n+1})^2 \underline{V}_n. \quad (2.19)$$

$$\underline{B}_{n+1} = \lambda_n {}^t \underline{V}_n. \quad (2.20)$$

$$(\underline{B}_{n+1})^{-1} = \underline{V}_n \lambda_n^{-1}. \quad (2.21)$$

$$|U_{n+1}\rangle = |r_n\rangle(\underline{B}_{n+1})^{-1}, \quad (2.22)$$

where the U -matrix is obtained as the expansion coefficients in the Lanczos vectors with respect to the non-orthogonal basis set. Inserting Eq. (2.12) and its variants into the identity $G(Z)(ZS - H) = I$ based on the non-orthogonal and the dual basis sets, we see that the Green's function matrix based on the dual basis set is connected with the Lanczos basis representation through the following relation:

$$G^D(Z) = UG^L(Z)^\dagger U. \quad (2.23)$$

While this transformation is apparently similar to Eq. (2.13), it should be noted that Eq. (2.13) is defined as the inverse transformation, since the transformation of the Green's function such as Eq. (3.51) is given by $G^L(Z) = {}^\dagger USG^D(Z)SU$.

Since ${}^\dagger USG^D(Z)SU = {}^\dagger UG(Z)U$ in the identity based on the Lanczos basis and the transformation is similar to that of the Hamiltonian, the Green's function based on the Lanczos basis can be directly connected with the Hamiltonian of the Lanczos basis representation through the identity $G(Z)(ZI - H) = I$, while the Hamiltonian based on the non-orthogonal basis is related to the Green's function based on the dual basis by the identity. The equality of the representation in the Lanczos basis is due to the orthogonality of the Lanczos basis.

As discussed the generalization of the block BOP above, although it would be hoped that the slight modifications in the non-orthogonal basis case cause outwardly no problems in terms of the computational efforts compared to the block BOP for the orthogonal basis case, however, the generalized block BOP possesses intrinsically several problems which discourage us applying the method to the non-orthogonal basis case as an efficient $O(N)$ method. The computational inefficiency may be caused by two calculations in the block BOP algorithm: the inverse of the overlap matrix which is essentially cubic in the scaling of the computation unless one uses any efficient scheme, and the transformation Eq. (2.23) of the Green's functions.

2.2.2 Analytic example

In order to clarify the inefficiency, as an illustration of the generalized block BOP we apply the method to the simplest system, i.e., a s-valent dimer. It is assumed that the dimer has two electrons, the hopping integrals is $-h(0 < h)$, the overlap is $S(0 < S)$, the on-site energies are zero, and the electronic temperature is zero. The inverse of the overlap matrix and the modified Hamiltonian is then given by

$$S^{-1} = \frac{1}{1 - S^2} \begin{pmatrix} 1 & -S \\ -S & 0 \end{pmatrix}. \quad (2.24)$$

$$H' = \frac{1}{1 - S^2} \begin{pmatrix} Sh & -h \\ -h & Sh \end{pmatrix}. \quad (2.25)$$

If the Lanczos algorithm Eqs. (2.15)-(2.22) is applied to the dimer with a site $|1\rangle$ which is a non-orthogonal basis as the starting state, as a result, the recursion coefficients are given

as $A_0 = 0$, $A_1 = 2Sh/(1 - S^2)$, and $B_1 = h/\sqrt{1 - S^2}$, and the U -matrix can be written as follows:

$$U = \begin{pmatrix} 1 & \frac{S}{\sqrt{1-S^2}} \\ 0 & \frac{-1}{\sqrt{1-S^2}} \end{pmatrix}. \quad (2.26)$$

Moreover, considering that the recursion coefficients and the identity, we get

$$G_{00}^L(Z) = \frac{\frac{1-S}{2}}{Z - \frac{h}{1-S}} + \frac{\frac{1+S}{2}}{Z + \frac{h}{1+S}}. \quad (2.27)$$

$$G_{01}^L(Z) = \frac{\frac{\sqrt{1-S^2}}{2}}{Z - \frac{h}{1-S}} + \frac{\frac{-\sqrt{1-S^2}}{2}}{Z + \frac{h}{1+S}}. \quad (2.28)$$

$$G_{11}^L(Z) = \frac{\frac{1+S}{2}}{Z - \frac{h}{1-S}} + \frac{\frac{1-S}{2}}{Z + \frac{h}{1+S}}, \quad (2.29)$$

where $G_{01}^L(Z) = G_{10}^L(Z)$. From Eq. (2.23) and the Green's functions based on the Lanczos basis, we have

$$G_{11}^D(Z) = G_{00}^L(Z) + 2\frac{S}{\sqrt{1-S^2}}G_{10}^L(Z) + \frac{S^2}{1-S^2}G_{11}^L(Z), \quad (2.30)$$

$$G_{12}^D(Z) = -\frac{1}{\sqrt{1-S^2}}G_{01}^L(Z) - \frac{S}{1-S^2}G_{11}^L(Z), \quad (2.31)$$

$$G_{22}^D(Z) = \frac{1}{1-S^2}G_{11}^L(Z), \quad (2.32)$$

where $G_{12}^D(Z) = G_{21}^D(Z)$. Thus, the bond-order matrix can be evaluated from the residues of the poles which are occupied in the Green's functions, namely

$$\Theta = \begin{pmatrix} \frac{1}{1+S} & \frac{1}{1+S} \\ \frac{1}{1+S} & \frac{1}{1+S} \end{pmatrix}. \quad (2.33)$$

The simple example clearly shows that the generalized block BOP requires huge computational efforts in practical applications compared with the block BOP in the orthogonal case, which discourages us applying the block BOP to large scale simulations as an efficient $O(N)$ method. The huge computational efforts can be produced by the Lanczos inverse transformation Eq. (2.23). In this transformation all the off-diagonal block elements are required in addition to \underline{G}_{0n}^L which are used in the orthogonal case, since the first block line of the U -matrix is not a zero line. It can be a considerably time-consuming step to evaluate all the off-diagonal elements in the Green's function matrix based on the Lanczos basis. Also the cubic computational efforts are required in evaluating the inverse of the overlap matrix.

2.3 Algorithm B

2.3.1 Formalism

Let us introduce a hybrid representation[56] of Hamiltonian which is a non Hermitian matrix represented by the original and the dual bases as $H'_{i\alpha,j\beta} = \langle i\tilde{\alpha}|\hat{H}|j\beta\rangle$. The hybrid Hamiltonian can be written in the matrix form as $H' = S^{-1}H$, where $H_{i\alpha,j\beta} \equiv \langle i\alpha|\hat{H}|j\beta\rangle$. With the relation $G(Z)(ZS - H) = I$, the hybrid Green function $G'(Z)$ defined by

$$G'_{i\alpha,j\beta}(Z) = \{G(Z)S\}_{i\alpha,j\beta} = \langle i\tilde{\alpha}|\hat{G}(Z)|j\beta\rangle \quad (2.34)$$

satisfies $G'(Z)(ZI - H') = I$. One of the merits of using $G'(Z)$ is that its diagonal element gives directly the Mulliken population $P_{i\alpha}$ of an orbital $|i\alpha\rangle$:

$$\begin{aligned} P_{i\alpha} &= -\frac{2}{\pi} \text{Im} \int G'_{i\alpha,i\alpha}(E + 0^+) f\left(\frac{E - \mu}{k_B T}\right) dE \\ &= \sum_{j\beta} \Theta_{i\alpha,j\beta} S_{j\beta,i\alpha}. \end{aligned} \quad (2.35)$$

In the block BOP, determination of the chemical potential is needed to conserve the total number of electrons N_{ele} in the system [13], so that the relation of Eq. (2.35) is very advantageous to computational efficiency because of the simple relation $N_{\text{ele}} = \sum_{i\alpha} P_{i\alpha}$. Thus, we present below a prescription how to calculate the hybrid Green functions. The diagonal elements of the Green function matrix can be calculated in a numerically stable way by the recursion method [33] based on the Lanczos algorithm [35]. The block BOP method is a general recursion method for evaluating efficiently both the diagonal and off-diagonal elements of the Green function matrix by the recursion method. Moreover the use of a single site containing all the localized orbitals as the starting state in the *block* Lanczos algorithm rather than a single orbital in the usual one conserves the rotational invariance of the total energy. In the present case of non-orthogonal basis, we further extend the formalism to adopt a two-sided block Lanczos algorithm [57], since the hybrid Hamiltonian is not any more Hermitian. The two-sided block Lanczos algorithm can be performed in the following procedure:

$$\underline{A}_n = (\tilde{U}_n|\hat{H}|U_n), \quad (2.36)$$

$$\begin{aligned} |r_n\rangle &= \hat{H}|U_n\rangle - |U_n\rangle\underline{A}_n - |U_{n-1}\rangle\underline{B}_n, \\ \langle\tilde{r}_n| &= \langle\tilde{U}_n|\hat{H} - \underline{A}_n\langle\tilde{U}_n| - \underline{C}_n\langle\tilde{U}_{n-1}|, \end{aligned} \quad (2.37)$$

$$\underline{B}_{n+1}\underline{C}_{n+1} = \langle\tilde{r}_n|r_n\rangle, \quad (2.38)$$

$$\begin{aligned} |U_{n+1}\rangle &= |r_n\rangle(\underline{C}_{n+1})^{-1}, \\ \langle\tilde{U}_{n+1}| &= (\underline{B}_{n+1})^{-1}\langle\tilde{r}_n|, \end{aligned} \quad (2.39)$$

\underline{A}_n , \underline{B}_n , and \underline{C}_n are recursion block coefficients with $M_i \times M_i$ in size, where M_i is the number of localized orbitals on the starting atom i , and the underline indicates that the element is

a block. In the two-sided block Lanczos algorithm the Lanczos vectors in the left and right sides have a bi-orthogonality relation. It is essential to start the two-sided block Lanczos algorithm with a single site and its corresponding dual state as

$$\begin{aligned} |U_0\rangle &= (|i1\rangle, |i2\rangle, \dots, |iM_i\rangle), \\ |\tilde{U}_0\rangle &= (|\tilde{i}1\rangle, |\tilde{i}2\rangle, \dots, |\tilde{i}M_i\rangle). \end{aligned} \quad (2.40)$$

Equation (2.40) is an optimum choice in terms of computational accuracy and efficiency because of the rotational invariance of the total energy and the consistent description for the different properties of σ , π , and δ bonds.

In the Lanczos basis representation the Hamiltonian H^L is block-tridiagonalized as a non Hermitian matrix and the Green function matrix $G^L(Z)$ is the inverse of the matrix $(ZI - H^L)$, so that the block diagonal element $\underline{G}_{00}^L(Z) = (\tilde{U}_0|\hat{G}|U_0)$ can be written explicitly in the form of the multiple inverse as follows:

$$\underline{G}_{\sigma,00}^L(Z) = [ZI - \underline{A}_{\sigma,0} - \underline{B}_{\sigma,1}[ZI - \underline{A}_{\sigma,1} - \underline{B}_{\sigma,2}[\dots]^{-1}\underline{C}_{\sigma,2}]^{-1}\underline{C}_{\sigma,1}]^{-1}, \quad (2.41)$$

where the index L indicates the representation based on the Lanczos basis. The off-diagonal elements of hybrid Green function matrix can be calculated by using a recurrence relation which can be derived basically along the same line as that described for the case of orthogonal basis [13]. The explicit expression consistent with Eqs. (2.36) and (2.40) is given below:

$$\underline{G}_{\sigma,0n}^L(Z) = \left(\underline{G}_{\sigma,0n-1}^L(Z)(ZI - \underline{A}_{n-1}) - \underline{G}_{\sigma,0n-2}^L(Z)\underline{B}_{\sigma,n-1} - \delta_{1n}\underline{I} \right) (\underline{C}_n)^{-1},$$

where δ is Kronecker's delta, and $\underline{G}_{0-1}(Z) = \underline{C}_0 = \underline{0}$. The block elements of the Green function matrix have the same relation to the bond-orders based on the Lanczos basis $\underline{\Theta}_{0n}^L$ as that of the dual basis representation. Therefore, we can obtain the bond orders through the following transformation:

$$\underline{\Theta}_{ij} = \sum_{n,k} \underline{\Theta}_{0n}^L \tilde{\underline{U}}_{nk} S_{kj}^{-1}, \quad (2.42)$$

where $\tilde{\underline{U}}_{nj}$ is defined by $\tilde{\underline{U}}_{nj} = (\tilde{U}_n(|j1\rangle, |j2\rangle, \dots, |jM_j\rangle)$. As a result of the simple inverse transformation Eq. (2.42), we only have to perform the evaluation and the integration of the Green functions of the 0th block line in the Lanczos basis representation, which means that the computational time of the algorithm is about two times longer compared to that of the orthogonal case [13]. Only the hybrid representation can provide this simple relation Eq. (2.42) as well as Eq. (2.35), while the other representations suffer from computational inefficiency [33, 58]. In the generalized block BOP using the non-orthogonal basis we need to calculate S^{-1} , the inverse of the overlap matrix. In the following calculations, we used a new $O(N)$ efficient method for inverting the overlap matrix [59].

2.3.2 Analytic example

We apply the algorithm B to the simplest system, i.e., a s-valent dimer. It is assumed that the dimer has two electrons, the hopping integrals is $-h(0 < h)$, the overlap is $S(0 < S)$,

the on-site energies are zero, and the electronic temperature is zero. So, we can write the Hamiltonian and overlap matrices as follows:

$$H = \begin{pmatrix} 0 & -h \\ -h & 0 \end{pmatrix}, \quad S = \begin{pmatrix} 1 & s \\ s & 1 \end{pmatrix}. \quad (2.43)$$

In this model, each atom has one basis orbital. So, the block algorithm becomes the scalar version. First, the Lanczos algorithm is applied to the overlap matrix to calculate the inverse of the overlap matrix. When the initial state is set as $\langle L_0^S | = (1, 0)$, we find that $a_0 = 1, a_1 = 1, b_1 = s$, and $\langle L_1^S | = (0, 1)$. Then, the diagonal element $R_{00}^L(Z)$ of the resolvent $R^L(Z) \equiv (S^L - ZI)^{-1}$ is written as

$$\begin{aligned} R_{00}^L(Z) &= \frac{1}{a_0 - Z - \frac{b_1^2}{a_1 - Z}} \\ &= \frac{1 - Z}{(1 - Z)^2 - s^2} \end{aligned} \quad (2.44)$$

Considering $R^L(Z)(S^L - ZI) = 1$, we have

$$\begin{aligned} R_{01}^L(Z) &= \frac{1}{b_1} \left(1 - (a_0 - Z)R_{00}^L(Z) \right) \\ &= \frac{-s}{(1 - Z)^2 - s^2} \end{aligned} \quad (2.45)$$

The resolvent based on the original representation $\{|1\rangle, |2\rangle\}$ is normally evaluated from the inverse transformation $R_{ij}(Z) = \sum_n R_{0n}^L {}^tU_{nj}$, where ${}^tU_{nj} = \langle L_n^S | j \rangle$. However, we find that $R(Z) = R^L(Z)$ in the simple model. So, the inverse of overlap matrix can be given using the resolvent as

$$\begin{aligned} S^{-1} &= \text{Re}R(0) \\ &= \frac{1}{1 - s^2} \begin{pmatrix} 1 & -s \\ -s & 1 \end{pmatrix}, \end{aligned} \quad (2.46)$$

After calculating the hybrid representation $H' = S^{-1}H$ of Hamiltonian using Eq. (2.46), we apply the two-sided Lanczos algorithm to H' . If assuming that $\langle L_0 | = (1, 0), \langle R_0 | = (1, 0)$ for the left and right initial Lanczos vectors, then we obtain the following recursion coefficients:

$$A_0 = A_1 = \frac{sh}{1 - s^2} \quad (2.47)$$

$$B_1 = C_1 = \frac{h}{1 - s^2} \quad (2.48)$$

$$(2.49)$$

Also, we find that $\langle L_1 | = (0, -1), \langle R_1 | = (0, -1)$ In the Lanczos representation, the diagonal $G_{00}^L(Z)$ and off-diagonal $G_{01}^L(Z)$ elements of Green's function $G^L(Z) \equiv (ZI - H^L)^{-1}$ are

given by

$$\begin{aligned}
G_{00}^L(Z) &= \frac{1}{Z - A_0 - \frac{B_1 C_1}{Z - A_1}} \\
&= \frac{\frac{1}{2}}{Z - \frac{h}{1-s}} + \frac{\frac{1}{2}}{Z + \frac{h}{1+s}}
\end{aligned} \tag{2.50}$$

$$\begin{aligned}
G_{01}^L(Z) &= \frac{1}{C_1} \left(G_{00}^L(Z)(Z - A_0) - 1 \right) \\
&= \frac{\frac{1}{2}}{Z - \frac{h}{1-s}} + \frac{-\frac{1}{2}}{Z + \frac{h}{1+s}}
\end{aligned} \tag{2.51}$$

Assuming that the total number of electron in the system is two, the density matrix based on the Lanczos representation is written as $\rho_{00}^L = 1/2$ and $\rho_{01}^L = -1/2$ by taking account of the residue in Eqs. (2.51) and (2.52). Applying the inverse transformation, then we have the density matrix based on the original representation:

$$\begin{aligned}
\rho_{11} &= \rho_{00}^L S_{11}^{-1} - \rho_{01}^L S_{21}^{-1} \\
&= \frac{1}{2(1+s)}
\end{aligned} \tag{2.52}$$

$$\begin{aligned}
\rho_{12} &= \rho_{00}^L S_{12}^{-1} - \rho_{01}^L S_{22}^{-1} \\
&= \frac{1}{2(1+s)}
\end{aligned} \tag{2.53}$$

$$\tag{2.54}$$

We see that the density matrix is equivalent to that by the usual diagonalization. For ρ_{22}, ρ_{21}^L of atom 2, the same procedure can be applied.

2.3.3 Numerical tests

In Fig. 2.1 we show convergence properties of the band energy in an insulator and a metal described by a simple s-valent TB as a test of the present method. The errors in the band energy at the seven-shell cluster and recursion levels are 0.2 % and 0.9 % for the insulator and the metal, respectively. Thus, we see that the block BOP gives sufficient convergent results in both the simple insulator and metal. Figures 2.2(a) and (b) show the error in the band energy at the five-shell cluster and recursion levels for insulators and metals described by a simple s-valent TB as a function of direct band gap and electronic temperature, respectively. In insulators the error goes to zero as the gap increases, while the errors, whose absolute values are no more than 0.5 % compared to the band energy in the whole region, are relatively small. In metals the error becomes almost negligible for the higher electronic temperature. This behavior in both insulators and metals is consistent with the recent study about the locality of the density matrix [60], though the block BOP depends on the convergence of the moment expansions for the density matrix rather than the locality of the density matrix [13]. From the comparison in the NaCl and FCC structures it is clear that the use of the terminator in the diagonal Green functions effectively reduces the error in both cases. Next we discuss

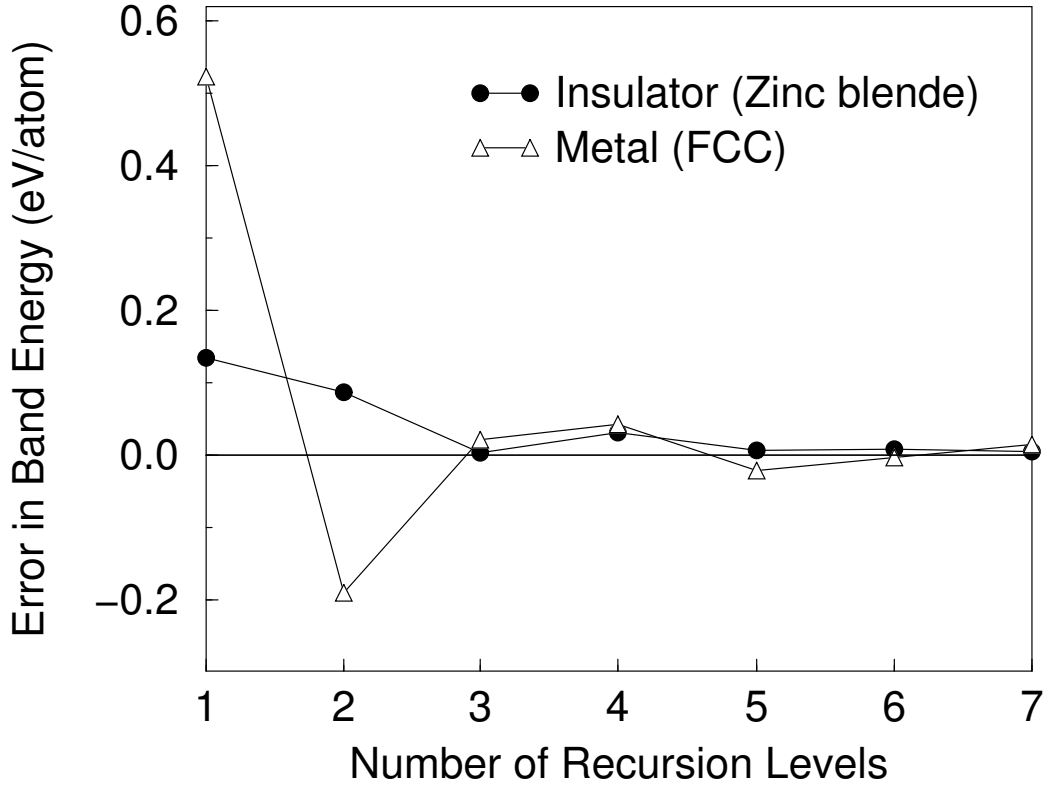


Figure 2.1: The error, with respect to the standard k-space calculations, in the band energy for an insulator (zinc blende) and a metal (FCC) described by a simple s-valent TB model in which the nearest neighbor hopping and overlap integrals are -1.0 eV and 0.1, respectively, with others being zero, and the number of electrons is the same as that of atoms. The zinc blende has a direct gap of 1.0 eV which was controlled by the gap of the on-site energies of the different atoms. In these calculations, the seven-shell cluster and a square-root terminator were used.

convergence properties of the block BOP in realistic materials within the TB based DFT proposed by Sankey and Niklewski [7]. Figure 2.3 shows the convergence properties of the cohesive energy for carbon in the diamond structure, silicon in the diamond structure, fcc aluminum, and C_{60} molecule. In carbon and silicon the cohesive energies rapidly converge to the k-space results in the five and seven-shell clusters, while the convergence values for the three-shell cluster are in error by 0.4 and 0.9 % from the k-space results, respectively. Even for metallic aluminum, the convergence is very fast with respect to the number of recursion levels and the errors in the converged values are only 0.3 and 0.1 % for the three- and five shell clusters, respectively. For C_{60} the convergence is achieved with the three-shell cluster. The error at the sixth recursion level is only 0.02 %.

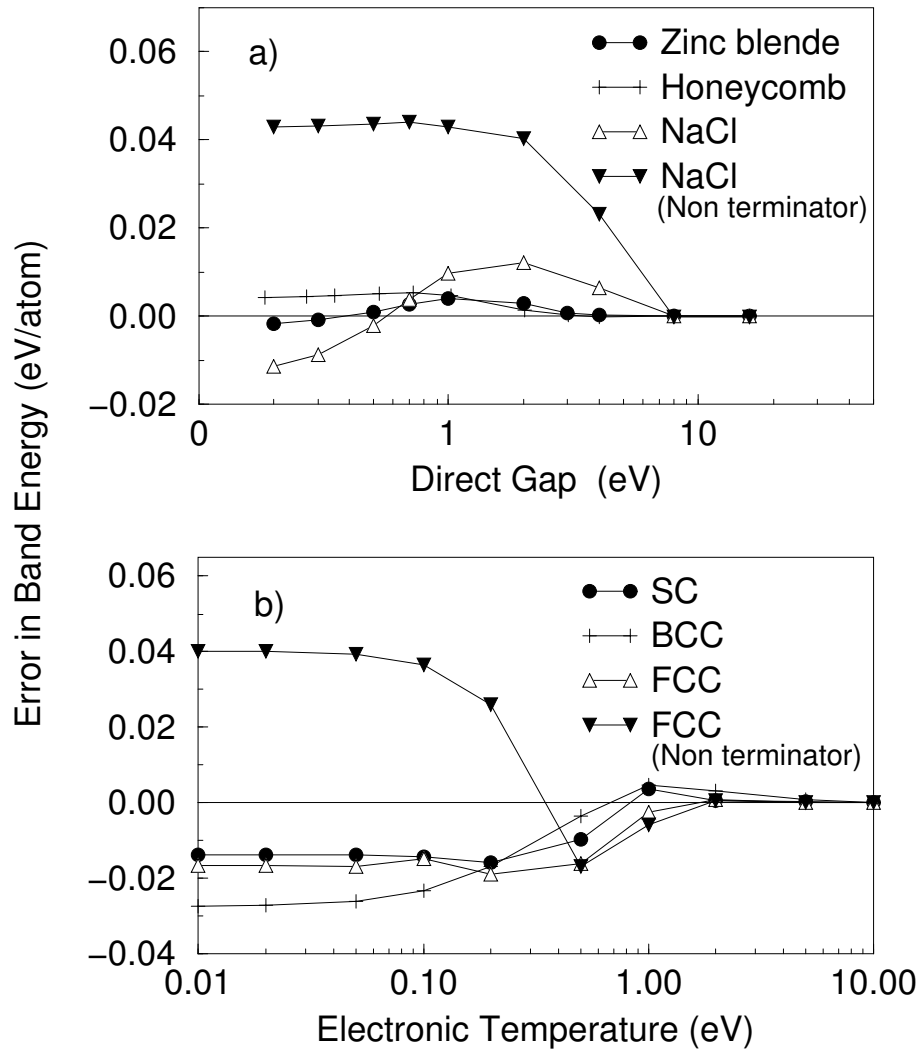


Figure 2.2: The error in the band energy for (a) insulators and (b) metals, calculated at the five-shell cluster and recursion levels. The calculations were carried out with the same s-valent TB model as that in Fig. 2.1 using a square-root terminator. For NaCl and FCC the non terminator results are also shown.

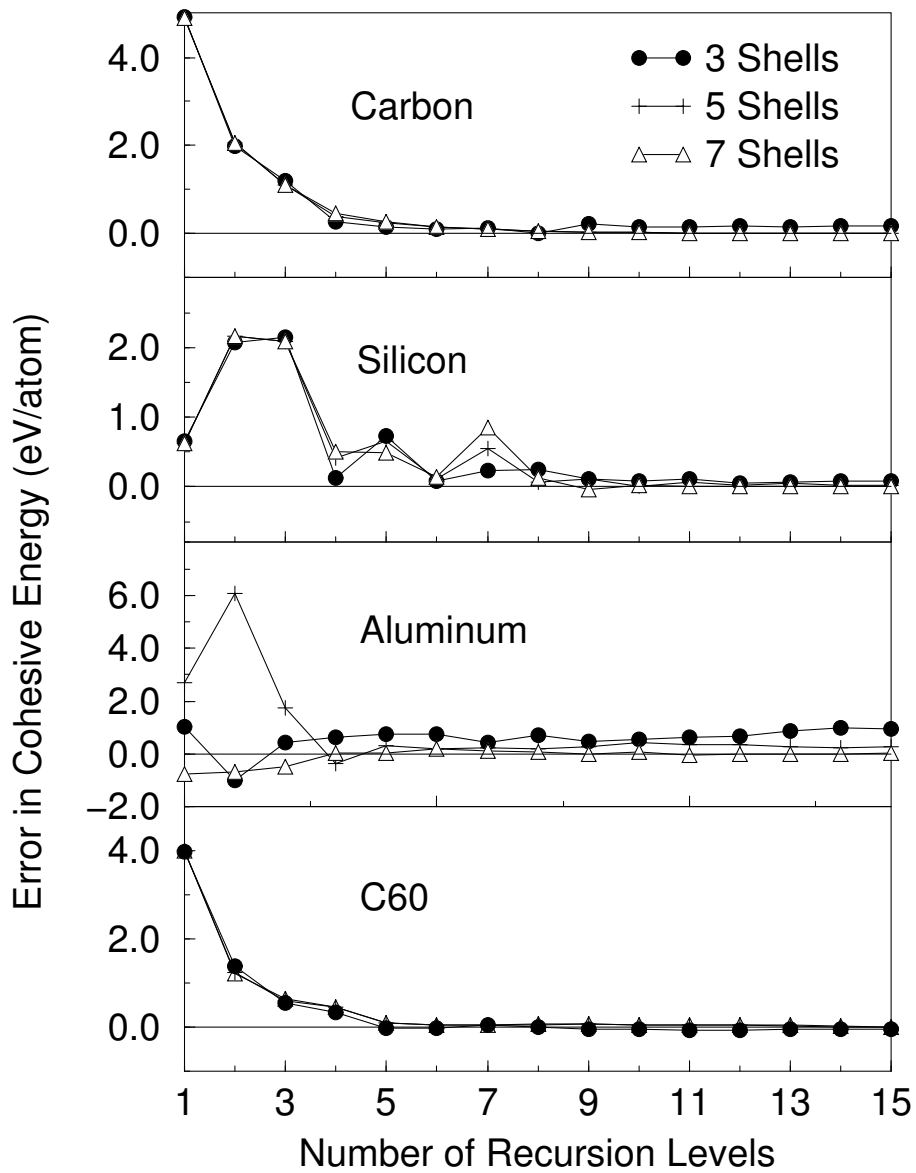


Figure 2.3: The error in the cohesive energy for carbon in the diamond structure, silicon in the diamond structure, fcc aluminum, and C₆₀ for three-, five-, and seven-shell clusters, calculated using a square-root terminator. These calculations were performed within DFT.

2.5 Algorithm D

2.5.1 Formalism

In addition to the Lanczos algorithm described in the algorithm B, to increase the numerical stability, we introduce the two-sided block Gram-Schmidt algorithm, which maintains the orthogonality relation among Lanczos vectors, and the singular value decomposition for $\underline{B}_{n+1}\underline{C}_{n+1}$, which is highly effective to avoid the break down in the Lanczos process. The Lanczos algorithm is given as:

$$\begin{aligned} |U_0\rangle &= (|i1\rangle, |i2\rangle, \dots, |iM_i\rangle), \\ |\tilde{U}_0\rangle &= (|\tilde{i}1\rangle, |\tilde{i}2\rangle, \dots, |\tilde{i}M_i\rangle). \end{aligned} \quad (2.67)$$

$$\underline{A}_n = (\tilde{U}_n | \hat{H} | U_n), \quad (2.68)$$

$$\begin{aligned} |r_n\rangle &= \hat{H}|U_n\rangle - |U_n\rangle\underline{A}_n - |U_{n-1}\rangle\underline{B}_n, \\ (\tilde{r}_n| &= (\tilde{U}_n|\hat{H} - \underline{A}_n(\tilde{U}_n| - \underline{C}_n(\tilde{U}_{n-1}|, \end{aligned} \quad (2.69)$$

$$\begin{aligned} |r_n\rangle &:= |r_n\rangle - \sum_{k=0}^n |U_k\rangle(\tilde{U}_k|r_n) \\ (\tilde{r}_n| &:= (\tilde{r}_n| - \sum_{k=0}^n (\tilde{r}_n|U_k\rangle)(\tilde{U}_k| \end{aligned} \quad (2.70)$$

$$\underline{B}_{n+1}\underline{C}_{n+1} = (\tilde{r}_n|r_n) = VWQ, \quad (2.71)$$

$$\begin{aligned} \underline{B}_{n+1} &= VW^{1/2}, \\ \underline{C}_{n+1} &= W^{1/2}Q \end{aligned} \quad (2.72)$$

$$\begin{aligned} |U_{n+1}\rangle &= |r_n\rangle(\underline{C}_{n+1})^{-1}, \\ (\tilde{U}_{n+1}| &= (\underline{B}_{n+1})^{-1}(\tilde{r}_n|, \end{aligned} \quad (2.73)$$

By applying the Lanczos algorithm to the Hamiltonian matrix, we have a block symmetric tridiagonalized Hamiltonian.

$$H^L = \begin{pmatrix} \underline{A}_0 & \underline{B}_1 & & & & \\ \underline{C}_1 & \underline{A}_1 & \underline{B}_2 & & & \\ & \cdots & \cdots & & & \\ & & \cdots & \cdots & & \\ & & & \underline{C}_{N-1} & \underline{A}_{N-1} & \underline{B}_N \\ & & & & \underline{C}_N & \underline{A}_N \end{pmatrix}. \quad (2.74)$$

In the algorithm D, we directly diagonalize the tridiagonalized Hamiltonian using the QR factorization and the inverse iterative method, although the Green's functions, which are

expressed by the multiple inverse and the recurrence relation, are used in the algorithm A to evaluate the density matrix. So, we have the following eigen value equation:

$$H^L W = W E, \quad (2.75)$$

where E is a diagonal matrix in which the diagonal elements are eigenvalues E_μ , and W is a matrix constructed from the eigenvectors. Then, the Green's function based on the Lanczos basis is explicitly written by the delta function:

$$G_{mn}^L(Z) = \sum_{\mu} W_{m,\mu} W_{n,\mu} \delta(Z - E_{\mu}). \quad (2.76)$$

The Green's functions based on the original dual basis are easily obtained from Eq. (2.23). Then, we can utilize the efficient relations Eqs. (2.35) and (2.42) in the hybrid representation.

2.6 Preliminary tests

Figure 2.2 shows that the norm of residual density matrix of a benzene molecule as a function of SCF iterations. We see that the algorithm C is most stable and accurate. I think that a highly accurate precision for $O(N)$ methods might be required to achieve the convergence for SCF calculations.

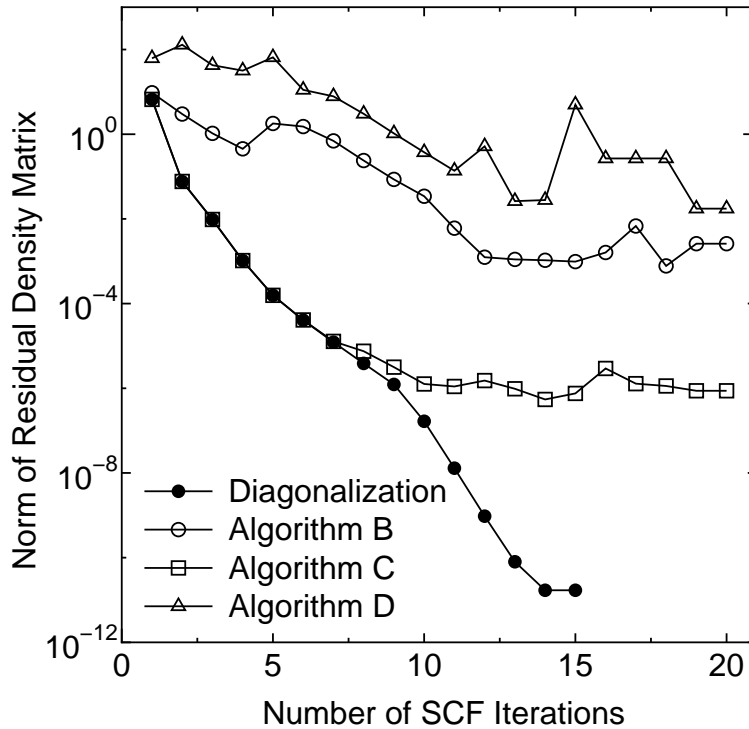


Figure 2.4: The norm of residual density matrix of a benzene molecule as a function of SCF iterations. The double valence basis sets are used for carbon and hydrogen atoms.

Appendix A

Modified Matsubara Summation

In this Appendix we give an efficient method for evaluating an integral with the Fermi function, which is required in the calculation of energies and response function, in addition, and an integral with the derivative of the Fermi function with respect to the chemical potential.

Although this is customarily performed in the complex plane by summing up an infinite series over the Matsubara poles, the convergence of this series is, however, very slow. A much more efficient scheme has been given by Nicholson et al. [40]. It should be noted that another scheme exists also[55].

It is possible to accelerate considerably the Matsubara summation by using the following approximant for the exponential function:

$$e^Z \approx \left(1 + \frac{Z}{n}\right)^n \quad (\text{A.1})$$

which becomes exact as n tends to infinity. This gives the following very useful representation for the Fermi function:

$$f(Z) = \frac{1}{e^{\beta(Z-\mu)} + 1} \approx \frac{1}{\left(1 + \frac{\beta(Z-\mu)}{2M}\right)^{2M} + 1}, \quad (\text{A.2})$$

where $\beta = 1/k_B T$, and μ is the chemical potential. This approximation has $2M$ simple poles (E_p) located on a circle in the complex plane off the real axis

$$E_p = \mu + \frac{2M}{\beta}(z_p - 1),$$

$$z_p = e^{\frac{i\pi(2p+1)}{2M}}, \quad p = 0, 1, \dots, 2M - 1. \quad (\text{A.3})$$

Therefore, assuming that $A(Z)$ defined in the complex plane is an analytical function inside the circles centered on the poles, the integral of a function $A(Z)$ with the Fermi function can be written as the sum of products between the function value $A(E_p)$ and the residues R_p for the poles E_p :

$$\int_{-\infty}^{\infty} A(E)f(E)dE \approx 2\pi i \sum_{p=0}^{M-1} A(E_p)R_p \quad (\text{A.4})$$

where R_p is given by

$$\begin{aligned} R_p &= \frac{1}{2\pi i} \oint_C f(Z) dZ \\ &= \frac{1}{2\pi} \lim_{r \rightarrow 0} \int_0^{2\pi} f(E_p + re^{i\theta}) re^{i\theta} d\theta, \end{aligned} \quad (\text{A.5})$$

where \oint_C reveals the path integral rotating counterclockwise around the poles E_p , and the second line was derived by transforming the variable as $Z = E_p + re^{i\theta}$. Expanding the approximated Fermi function using the binomial theorem, we get

$$\begin{aligned} \lim_{r \rightarrow 0} \int_0^{2\pi} f(E_p + re^{i\theta}) re^{i\theta} d\theta &= \lim_{r \rightarrow 0} \int_0^{2\pi} \frac{1}{\beta z_p^{2M-1} + \frac{2M-1}{4M} \beta^2 z_p^{2M-2} r e^{i\theta} + \dots} d\theta \\ &= -\frac{2\pi z_p}{\beta}. \end{aligned} \quad (\text{A.6})$$

Substituting Eq. (A.6) into Eq. (A.5), we get

$$R_p = -\frac{z_p}{\beta}. \quad (\text{A.7})$$

Thus, substituting Eq. (A.7) into Eq. (A.4) and dividing it into the real and imaginary parts, we have

$$\text{Re} \int_{-\infty}^{\infty} A(E) f(E) dE \approx \frac{2\pi}{\beta} \text{Im} \left[\sum_{p=0}^{M-1} z_p A(E_p) \right]. \quad (\text{A.8})$$

$$\text{Im} \int_{-\infty}^{\infty} A(E) f(E) dE \approx -\frac{2\pi}{\beta} \text{Re} \left[\sum_{p=0}^{M-1} z_p A(E_p) \right]. \quad (\text{A.9})$$

In case the numerical integral is applied to the Green's functions, we find that typically 30 to 50 complex poles are enough to achieve convergence within about 10 digits.

Next we consider an integral with the derivative of the Fermi function with respect to the chemical potential μ , which is required in the modified force approach discussed in chapter 3. Approximating the derivative using the same approximant Eq. (A.1) compared to the Fermi function case, we can write

$$\begin{aligned} \frac{\partial f(Z)}{\partial \mu} &= \frac{\beta e^{\beta(Z-\mu)}}{(e^{\beta(Z-\mu)} + 1)^2} = \beta \left(\frac{e^{\beta(Z-\mu)} + 1 - 1}{(e^{\beta(Z-\mu)} + 1)^2} \right) \\ &= \beta \left(\frac{1}{e^{\beta(Z-\mu)} + 1} - \frac{1}{(e^{\beta(Z-\mu)} + 1)^2} \right) \\ &\approx \sum_{p=0}^{2M-1} \frac{-z_p}{Z - E_p} + \sum_{p,p'=0}^{2M-1} \frac{-\frac{z_p z_{p'}}{\beta}}{(Z - E_p)(Z - E_{p'})}. \end{aligned} \quad (\text{A.10})$$

This approximation has $2M$ poles (E_p) to the second order which are located on the circle in the complex plane similar to the approximated Fermi function. The second term of the

right side in Eq. (A.10) can be decomposed into the sum of partial fractions as follows:

$$\sum_{p,p'=0}^{2M-1} -\frac{\frac{z_p z_{p'}}{\beta}}{(Z - E_p)(Z - E_{p'})} = \frac{1}{M} \sum_{p=0}^{2M-1} \frac{z_p}{Z - E_p} \left(\sum_{p' \neq p}^{2M-1} \frac{z_{p'}}{z_p - z_{p'}} \right) + \sum_{p=0}^{2M-1} \frac{\frac{z_p^2}{\beta}}{(Z - E_p)^2}. \quad (\text{A.11})$$

The sum in the parenthesis of Eq. (A.11) can be simplified as follows:

$$\begin{aligned} \sum_{p' \neq p}^{2M-1} \frac{z_{p'}}{z_p - z_{p'}} &= \sum_{p' \neq p}^{2M-1} \frac{1}{e^{\frac{i\pi(p-p')}{M}} - 1} \\ &= \sum_{p=1}^{2M-1} \frac{1}{e^{\frac{i\pi p}{M}} - 1} \\ &= \sum_{p=1}^{2M-1} \frac{1}{\left(\cos \frac{p}{M}\pi - 1\right) + i \sin \frac{p}{M}\pi} \\ &= -\sum_{p=1}^{2M-1} \frac{1}{2} + i \sum_{p=1}^{2M-1} \frac{\sin \frac{p}{M}\pi}{\cos \frac{p}{M}\pi - 1}. \end{aligned} \quad (\text{A.12})$$

The imaginary part in Eq. (A.12) is zero due to the unsymmetrical summation for $p = M$, so that we get a very simple result for the sum in the parenthesis of Eq. (A.11):

$$\sum_{p' \neq p}^{2M-1} \frac{z_{p'}}{z_p - z_{p'}} = -M + \frac{1}{2}. \quad (\text{A.13})$$

Substituting Eq. (A.13) into Eqs. (A.11) and (A.10) we have

$$\frac{\partial f(Z)}{\partial \mu} \approx -\frac{1}{2M} \sum_{p=0}^{2M-1} \frac{z_p}{Z - E_p} - \frac{1}{\beta} \sum_{p=0}^{2M-1} \frac{z_p^2}{(Z - E_p)^2}. \quad (\text{A.14})$$

Thus, the integral of the block element $\underline{G}_{00}(Z)$ with the approximated derivative Eq. (A.14) can be written as follows:

$$\text{Re} \int_{-\infty}^{\infty} \underline{G}_{00}(E) \frac{\partial f(E)}{\partial \mu} dE \approx \frac{\pi}{M} \text{Im} \left[\sum_{p=0}^{M-1} z_p \underline{G}_{00}(E_p) \right] + \frac{2\pi}{\beta} \text{Im} \left[\sum_{p=0}^{M-1} z_p^2 \underline{G}'_{00}(E_p) \right]. \quad (\text{A.15})$$

$$\text{Im} \int_{-\infty}^{\infty} \underline{G}_{00}(E) \frac{\partial f(E)}{\partial \mu} dE \approx -\frac{\pi}{M} \text{Re} \left[\sum_{p=0}^{M-1} z_p \underline{G}_{00}(E_p) \right] - \frac{2\pi}{\beta} \text{Re} \left[\sum_{p=0}^{M-1} z_p^2 \underline{G}'_{00}(E_p) \right] \quad (\text{A.16})$$

with $G'(E_p)$ which is a function value at E_p for the derivative of $G(Z)$ with respect to Z calculated by

$$\underline{G}'_{00}(E_p) = -\sum_{n=0} G_{0n}(E_p) G_{n0}(E_p). \quad (\text{A.17})$$

The relation Eq. (A.17) is derived from the identity based on the Lanczos basis representation. Also the integral of the product between E and the block element $\underline{G}_{00}(Z)$ with the approximated derivative Eq. (A.14) can be written as follows:

$$\begin{aligned} & \operatorname{Re} \int_{-\infty}^{\infty} E \underline{G}_{00}(E) \frac{\partial f(E)}{\partial \mu} dE \\ & \approx \frac{\pi}{M} \operatorname{Im} \left[\sum_{p=0}^{M-1} z_p E_p \underline{G}_{00}(E_p) \right] + \frac{2\pi}{M} \operatorname{Im} \left[\sum_{p=0}^{M-1} z_p^2 \underline{G}_{00}(E_p) \right] - \frac{2\pi}{\beta} \operatorname{Im} \left[\sum_{p=0}^{M-1} z_p^2 E_p \underline{G}'_{00}(E_p) \right]. \end{aligned} \quad (\text{A.18})$$

$$\begin{aligned} & \operatorname{Im} \int_{-\infty}^{\infty} E \underline{G}_{00}(E) \frac{\partial f(E)}{\partial \mu} dE \\ & \approx -\frac{\pi}{M} \operatorname{Re} \left[\sum_{p=0}^{M-1} z_p E_p \underline{G}_{00}(E_p) \right] - \frac{2\pi}{M} \operatorname{Re} \left[\sum_{p=0}^{M-1} z_p^2 \underline{G}_{00}(E_p) \right] + \frac{2\pi}{\beta} \operatorname{Re} \left[\sum_{p=0}^{M-1} z_p^2 E_p \underline{G}'_{00}(E_p) \right]. \end{aligned} \quad (\text{A.19})$$

These expressions Eqs. (A.18) and (A.19) have been derived for the first time in this Appendix.

Bibliography

- [1] R. McWeeny, *Methods of Molecular Quantum Mechanics*, 1989, (Academic Press, New York).
- [2] P. Fulde, *Electron Correlations in Molecules and Solids*, 1995, (Springer Series in Solid-State Sciences, Vol 100).
- [3] B. L. Hammond, W. A. Lester, and P. J. Reynolds, 1994, *Monte Carlo Methods in Ab Initio Quantum Chemistry*, (World Scientific).
- [4] M. K. Gilson, J. A. McCammon, and J. D. Madura, *J. Comp. Chem.* **16**, 1081 (1995).
- [5] S. T. Wlodek, J. Antosiewicz, and J. A. McCammon, *Protein Sci.* **6**, 373 (1997).
- [6] W. Kohn and L. J. Sham, *Phys. Rev. B* **140**, A1133 (1965).
- [7] O. F. Sankey and D. J. Niklewski, *Phys. Rev. B* **40**, 3979 (1989).
- [8] A. P. Horsfield, *Phys. Rev. B* **56**, 6594 (1997).
- [9] J. C. Slater and G. F. Koster, *Phys. Rev.* **94**, 1498 (1954).
- [10] A. P. Sutton, M. W. Finnis, D. G. Pettifor, and Y. Ohta, *J. Phys. C* **21**, 35 (1988).
- [11] D. G. Pettifor, *Phys. Rev. Lett.* **63**, 2480 (1989).
- [12] M. Aoki, *Phys. Rev. Lett.* **71**, 3842 (1993).
- [13] T. Ozaki, *Phys. Rev. B* **59**, 16061 (1999); T. Ozaki, M. Aoki, and D. G. Pettifor, submitted to *Phys. Rev. B* (cond-mat/9909064).
- [14] A. P. Horsfield, A. M. Bratkovsky, D. G. Pettifor, and M. Aoki, *Phys. Rev. B* **53**, 1656 (1996).
- [15] A. P. Horsfield, A. M. Bratkovsky, M. Fearn, D. G. Pettifor, and M. Aoki, *Phys. Rev. B* **53**, 12694 (1996).
- [16] S. Goedecker and L. Colombo, *Phys. Rev. Lett.* **73**, 122 (1994).
- [17] S. Goedecker and M. Teter, *Phys. Rev. B* **51**, 9455 (1995).
- [18] W. T. Yang, *Phys. Rev. Lett.* **66**, 1438 (1991).
- [19] G. Galli and M. Parrinello, *Phys. Rev. Lett.* **69**, 3547 (1992).

- [20] F. Mauri, G. Galli, and R. Car, Phys. Rev. B **47**, 9973 (1993).
- [21] F. Mauri and G. Galli, Phys. Rev. B **50**, 4316 (1994).
- [22] X.-P. Li, R. W. Nunes, and D. Vanderbilt, Phys. Rev. B **47**, 10891 (1993).
- [23] M. S. Daw, Phys. Rev. B **47**, 10895 (1993).
- [24] G. Galli and F. Mauri, Phys. Rev. Lett. **73**, 3471 (1994).
- [25] A. Canning, G. Galli, and J. Kim, Phys. Rev. Lett. **78**, 4442 (1997).
- [26] S. Goedecker, Rev. of Mod. Phys. **71**, 1085 (1999).
- [27] D. R. Bowler, M. Aoki, C. M. Goringe, A. P. Horsfield, and D. G. Pettifor, Modelling Simul. Mater. Sci. Eng. **5**, 199 (1997).
- [28] J. D. Kress and A. F. Voter, Phys. Rev. B **52**, 8766 (1995).
- [29] A. F. Voter, J. D. Kress, and R. N. Silver, Phys. Rev. B **53**, 12733 (1996).
- [30] A. P. Horsfield, Mater. Sci. Eng. **B37**, 219 (1996).
- [31] V. Heine, Solid State Phys. **35**, 1 (1980).
- [32] D. G. Pettifor, *Bonding and Structure of Molecules and Solids* (Oxford University Press, Oxford, 1995).
- [33] R. Haydock, V. Heine, and M. J. Kelly, J. Phys. C **5**, 2845 (1972); **8**, 2591 (1975).
- [34] R. Haydock, Solid State Phys. **35**, 216 (1980).
- [35] C. Lanczos, J. Res. Natl. Bur. Stand. **45**, 225 (1950).
- [36] R. Jones and M. W. Lewis, Philos. Mag. B **49**, 95 (1984).
- [37] J. Inoue and Y. Ohta, J. Phys. C **20**, 1947 (1987).
- [38] D. C. Lay, Linear Algebra and Its Applications (Addison-Wesley Publishing Company, 1994).
- [39] G. Golub and C. F. Van Loan, Matrix Computations (Johns Hopkins University Press, Baltimore, MD, third ed., 1996).
- [40] D. M. C. Nicholson, G. M. Stocks, Y. Wang, and W. A. Shelton, Phys. Rev. B **50**, 14686 (1994).
- [41] C. H. Xu, C. Z. Wang, C. T. Chan, and K. M. Ho, J. Phys. Condens. Matter **4**, 6047 (1992).
- [42] L. Goodwin, A. J. Skinner, and D. G. Pettifor, Europhys. Lett. **9**, 701 (1989).
- [43] A. P. Horsfield, P. D. Godwin, D. G. Pettifor, and A. P. Sutton, Phys. Rev. B **54**, 15773 (1996).

- [44] D. R. Bowler and M. J. Gillan (unpublished).
- [45] W. Yang, Phys. Rev. Lett. **66**, 1438 (1991); S. Goedecker and L. Colombo, Phys. Rev. Lett. **73**, 122 (1994); G. Galli and M. Parrinello, Phys. Rev. Lett. **69**, 3547 (1992); F. Mauri, G. Galli, and R. Car, Phys. Rev. B **47**, 9973 (1993); X.-P. Li, R. W. Nunes, and D. Vanderbilt, Phys. Rev. B **47**, 10891 (1993); M. S. Daw, Phys. Rev. B **47**, 10895 (1993); S. Goedecker, Rev. of Mod. Phys. **71**, 1085 (1999) and references therein.
- [46] S. D. Kenny, A. P. Horsfield, and H. Fujitani, Phys. Rev. B **62**, 4899 (2000).
- [47] J. Junquera, Ó. Paz, D. Sánchez-Portal, and E. Artacho, Phys. Rev. B **64**, 235111 (2001); J. M. Soler et al., J. Phys.:Condens. Matter **14**, 2745 (2002) and references therein.
- [48] C. K. Gan, P. D. Haynes, and M. C. Payne, Phys. Rev. B **63**, 205109 (2001).
- [49] J. D. Talman, Phys. Rev. Lett. **84**, 855 (2000).
- [50] G. B. Bachelet, D. R. Hamann, and M. Schlüter, Phys. Rev. B **26**, 4199 (1982); L. Kleinman and D. M. Bylander, Phys. Rev. Lett. **48**, 1425 (1982).
- [51] J. P. Perdew and A. Zunger, Phys. Rev. B **23**, 5048 (1981).
- [52] V. Barone, C. Adamo, and F. Lelj, J. Chem. Phys. **102**, 364 (1995).
- [53] K. Iijima, K. Tanaka, and S. Onuma, J. Mol. Struct. **246**, 257 (1991).
- [54] A. Warshel and M. Karplus, J. Am. Chem. Soc. **94**, 5612 (1972).
- [55] S. Goedecker, Phys. Rev. B **48**, 17573(1993).
- [56] T. Ozaki and K. Terakura, Phys. Rev. B **64**, 195126 (2001);
- [57] Z. Bai, D. Day, and Q. Ye, Siam J. Matrix Anal. Appl. **20**, 1060 (1999) and references therein.
- [58] A. Gibson, R. Haydock, and J. P. LaFemina, Phys. Rev. B **47**, 9229 (1993).
- [59] T. Ozaki, Phys. Rev. B **64**, 195110 (2001).
- [60] S. Ismail-Beigi and T. Arias, Phys. Rev. Lett. **82**, 2127 (1999).